ELSEVIER

Deep-Sea Research II 52 (2005) 2275–2301

DEEP-SEA RESEARCH
PART II

www.elsevier.com/locate/dsr2

Ice-rafted debris (IRD)-based sea-ice expansion events during the past 100 kyrs in the Okhotsk Sea

Tatsuhiko Sakamoto[a,*], M. Ikehara[b], K. Aoki[c], K. Iijima[a], N. Kimura[d], T. Nakatsuka[d], M. Wakatsuchi[d]

[a]*Institute For Research on Earth Evolution (IFREE), Japan Agency for Marine-Earth Science and Technology (JAMSTEC), Yokosuka 237-0061, Japan*
[b]*Center of Advanced Marine Core Research, Kochi University, 783-8502, Japan*
[c]*National Institute of Advanced Industrial Science and Technology, Tsukuba 305-8567, Japan*
[d]*Institute of low temperature Science, Hokkaido University, Sapporo 060-0819, Japan*

Received 1 June 2005; accepted 5 August 2005
Available online 21 October 2005

Abstract

Ice-rafted debris (IRD) from sediment traps, surficial sediments, and sediment cores were investigated in order to reconstruct the extent history of sea-ice cover during the last 100 kyrs in the Okhotsk Sea. The seasonal IRD buried into the sediments, during and just after sea-ice melting in spring, consists of silt- and sand- size terrigenous particles. The spatial distribution of IRD within surficial sediments clearly corresponds to the extent of sea-ice coverage. Sea-ice expanded to a maximum extent during the glacial periods, although sea-ice cover was not perennial. The Okhotsk Sea Sea-ice Expansion (OSIE) events, which are recognized by millennial-scale-abrupt peaks of IRD content, have occurred 13 times during the past 100 kyrs. These events were amplified during the glacial periods. A significant modification of the polar atmospheric circulation in the northern hemisphere is a key process in explaining these OSIE events.

Keywords: Okhotsk Sea; Sea-ice; Ice-rafted debris

1. Introduction

Expansion of seasonal sea-ice cover in the Okhotsk Sea has corresponded considerably to global and regional climatic changes. The seasonal sea-ice cover has a positive feedback effect on the climatic system by its high albedo and inhibitive effects on heat conductivity between the atmosphere and ocean. In addition, the formation of sea-ice has a significant influence on thermohaline circulation since dense and saline water (brine water) forms simultaneously. It is proposed that the water mass in the Okhotsk Sea is one of the possible sources of the North Pacific Intermediate Water (NPIW) (Talley, 1991; Watanabe and Wakatsuchi, 1998) and glacial Pacific-deep water (Duplessy et al., 1998; Talley, 1991; Zahn et al., 1991; Keigwin et al., 1998; Itou et al., 2003). Therefore, the Okhotsk Sea has played an important role in global and regional marine environments and climate changes.

*Corresponding author. Tel.: +81 46 867 9803; fax: +81 46 867 9775.
E-mail address: tats-ron@jamstec.go.jp (T. Sakamoto).

0967-0645/$ - see front matter © 2005 Elsevier Ltd. All rights reserved.
doi:10.1016/j.dsr2.2005.08.007

The Okhotsk Sea is characterized by the largest seasonal sea-ice coverage in the middle-latitude of the northern hemisphere. Sea-ice generally starts to form in November in the northern Okhotsk Sea. It repeatedly drifts southward under winter wind field and continually forms in polynya. Sea-ice covers much of the Okhotsk Sea in March with a thickness of ~1 m. It entirely disappears by the beginning of June. The sea is usually free of sea-ice for about 4 months from July to October (Parkinson et al., 1987). The information from satellite imagery demonstrates annual variability, both in the geographic extent and in seasonal duration of sea-ice cover (Parkinson et al., 1987; Alfulis and Martin, 1987; Gloerson et al., 1992). The formation, advance, and retreat of sea-ice are influenced by oceanographic and metrological factors, e.g., sea-ice advection and advance can be controlled by wind. Both wind and air temperature conditions are main factors in controlling the inter-annual variation in the maximum sea-ice coverage (Kimura and Wakatsuchi, 1999). This region provides us a great opportunity to understand the relationship between sea-ice and climate both in modern conditions and in longer time scales such as Milankovitch orbital and Dansgard-Oeschger cycles (e.g., Takahashi, 1998).

Ice-rafted debris (IRD), defined here as a series of terrigenous grains that are transported by drifted ice, are one of many useful paleoceanographic proxies to reconstruct sea-ice history from marine sediments. Terrigenous clastic grains are incorporated into sea-ice and icebergs through fluvial supply, coastal suspension freezing, cliff-fall and so on. In the seasonal sea-ice area, especially, the grains are caught into sea-ice during coastal suspension freezing and when sea-ice grounded near coastline on continental shelf. The grains are subsequently transported far away from land to sea by drifting sea-ice and icebergs. Before using IRD as a sea-ice proxy in a particular region, however, it is necessary to understand modern IRD sedimentation processes and the range of grain sizes and minerals, which are actually included in IRD.

In this paper, we outline modern IRD sedimentation processes in the Okhotsk Sea as constrained by sediment trap experiments. We have used these observations to reconstruct the spatial and temporal (millennium to glacial–interglacial scale) variations of sea-ice cover during the past 100 kyrs. Finally, we discuss millennium-scale sudden and abrupt cooling events in the Okhotsk Sea. The local millennium scale fluctuations in the Okhotsk Sea will provide an insight into reconstruction of atmospheric circulation intensity in the Northern Hemisphere.

2. Modern and paleo-oceanography

The Okhotsk Sea is a marginal sea, bounded by the Siberia, Sakhalin and Hokkaido Islands, the Kamchatka Peninsula, and the Kuril Islands chain. It has a variable seasonality with mild summers and cold, windy winters with sea-ice cover. In spite of its mid-latitude location, the climatic conditions are comparable to those of a polar ocean (Alfulis and Martin, 1987; Wakatsuchi and Martin, 1991). The surface waters circulate as a large cyclonic gyre consisting of two major currents (Alfulis and Martin, 1987). The northward surface and subsurface flow, called the West Kamchatka Current (WKC), originates from warm and saline Pacific water through two deep straits located in the Kuril Island chain, namely the Bussol' Strait (2300 m water depth) and Kuruzenshterna Strait (1900 m water depth). The WKC flows along the Kamchatka Peninsula and deviates to the west in the northern Okhotsk Sea, where it mixes with abundant fresh water discharged from the Amur River. The southward-flowing current along the Sakhalin Island is called the Eastern Sakhalin Current (ESC). Two shallow straits connect the Okhotsk Sea and the Japan Sea; the Soya Strait (40 m water depth), south of the Sakhalin Island, and the Tartar Strait (10 m water depth), north of Sakhalin. The Soya Warm Current (SWC) is characterized by warm and saline surface water, which is an extension of the eastward flowing Tsushima Warm Current. After mixing of the ESC and SWC in early spring, the surface current flows out of the Kuril Basin through the Bussol' Strait into the Pacific.

Throughout the entire basin at depths between 150 and 800 m, the water is characterized by cold, low-salinity, and oxygen-rich water, termed the Okhotsk Sea Intermediate Water (OSIW), and this water mass has the same density of the North Pacific water mass (Morley and Hays, 1983; Yang and Honjo, 1996). Sea-ice generation, subsequent brine release, and mixing with the Soya Warm Water are thought to be major contributors to the modern NPIW (Watanabe and Wakatsuchi, 1998; Itou et al., 2003). Itoh et al. (2003) showed that there are three ventilation sources for the formation of the OSIW: Dense Shelf Water (DSW) with cold and fresh properties influenced by sea-ice formation

in the northwest shelf region, the Forerunner of Soya Warm Current Water (FSCW), which has warm and saline properties originating in the Japan Sea, and the Western Subarctic Water (WSAW) originating from the North Pacific. They estimated the mixing ratio of 1:1:0.1 among the DSW, WSAW, and FSCW to form the OSIW by assuming of isopycnal mixing.

In spite of the importance of the global climate system, the paleoceanographic history of the Okhotsk Sea is not fully understood. Gorbarenko (1996) reported that $\delta^{13}C$ records of sediment cores from the Okhotsk Sea, Bering Sea, and the NW Pacific contradicted established models for increased intermediate water formation in the region during the glaciations. Keigwin (1998) suggested that the water-column properties at intermediate depths within the Okhotsk Sea and northwestern Pacific were similar and that these waters pass into the North Pacific Ocean providing a source of low salinity. Keigwin (1998) applied modern oxygen and carbon isotope values to the glacial benthic foraminifers and suggested that a well-ventilated modern intermediate and deep-water masses in the Okhotsk Sea were as old as that of the glacial northwestern Pacific. Ternois et al. (2000) estimated the alkenone sea-surface temperatures for the early deglaciation (15 kyrs BP) to be ~5 °C lower than today. Shiga and Koizumi (2000) demonstrated that open water existed in the eastern Okhotsk Sea and that perennial ice cover existed in the western part during the last glacial maximum, allowing heat exchange between the water and atmosphere through the surface layer. Matsumoto et al. (2002) compiled previous literature and discussed a potential for deepwater formation around the NW Pacific during the glacial, and termed the glacial North Pacific Intermediate Water (GNPIW). The origin of the GNPIW is still under debate. The glacial NW Pacific may have had water masses from the Okhotsk Sea and the south which was the glacial North Pacific Antarctic Intermediate Water (GNAIW). Such a mixture of the water masses may have been a source of the GNPIW formation.

3. Materials and methods

Settling particles and sea floor sediments were collected during Cruises XP-98, XP-99, and XP-00 on board R./V. *Professor Khromov* under a collaboration of Japan, Russia, and the US (Fig. 1, Table 1). Additional sets of sea floor sediments were retrieved during Cruise of GH-00 on board R./V. *Hakurei-maru* of AIST and Cruise MR00-K3 on board R./V. *Mirai* of JAMSTEC.

3.1. Sediment traps samples

Four time-series sediment traps (PARFLUX McLane Mark 78G-21 with 21 sampling cups) were deployed at Sites M4 and M6 located off Sakhalin Island from August 1998 through July 2000 (Fig. 1). The shallow and deep traps were set at water depths of 300 and 1550 m at Site M4, and at 300 and 700 m at Site M6, respectively. Each sampling cup was filled with a 5% formaldehyde solution buffered with sodium borate in filtered seawater in order to eliminate in situ biological degradation. The total terrigenous flux in each sample cup of sediment traps was measured by residual weight after the removal of all of organic materials by a procedure mentioned in Section 3.3. The residual terrigenous grains were observed on filtered trap samples under the stereoscope.

Sea-ice concentration during the sediment trap mooring was calculated by a modified NASA algorithm (Kimura and Wakatsuchi, 1999) from the brightness temperature of DMSP SSM/I.

3.2. Surface sediments and sediment core samples

Surface sediments and sediment cores were collected using multiple and piston corer systems (Table 1). Sediment Cores XP-PC1 (1010.0 cm in recovered length, 1107 m water depth), XP-PC2 (1023.0 cm in recovered length, 1258 m water depth), and XP-PC4 (1128.0 cm in recovered length, 664 m water depth) were used in this study. Sediment samples were taken from Core XP-PC1 with a 1.2 cm interval and from Cores XP-PC2 and XP-PC4 with a 2.4 cm interval. Samples were stored at 3 °C until the shore-based analysis was performed. The sediments mainly consist of grayish-olive, homogenous and bioturbated diatom ooze and diatomaceous clayey silt. Occasional tephra layers form an interbedded component of the cores. Dropstones (>2 mm in diameter) were often found in cores.

3.3. Grain size and mineral assemblage analyses

After removing calcium carbonate by acidification from aliquot samples of sediment trap samples, surficial sediments, and sediment cores, organic

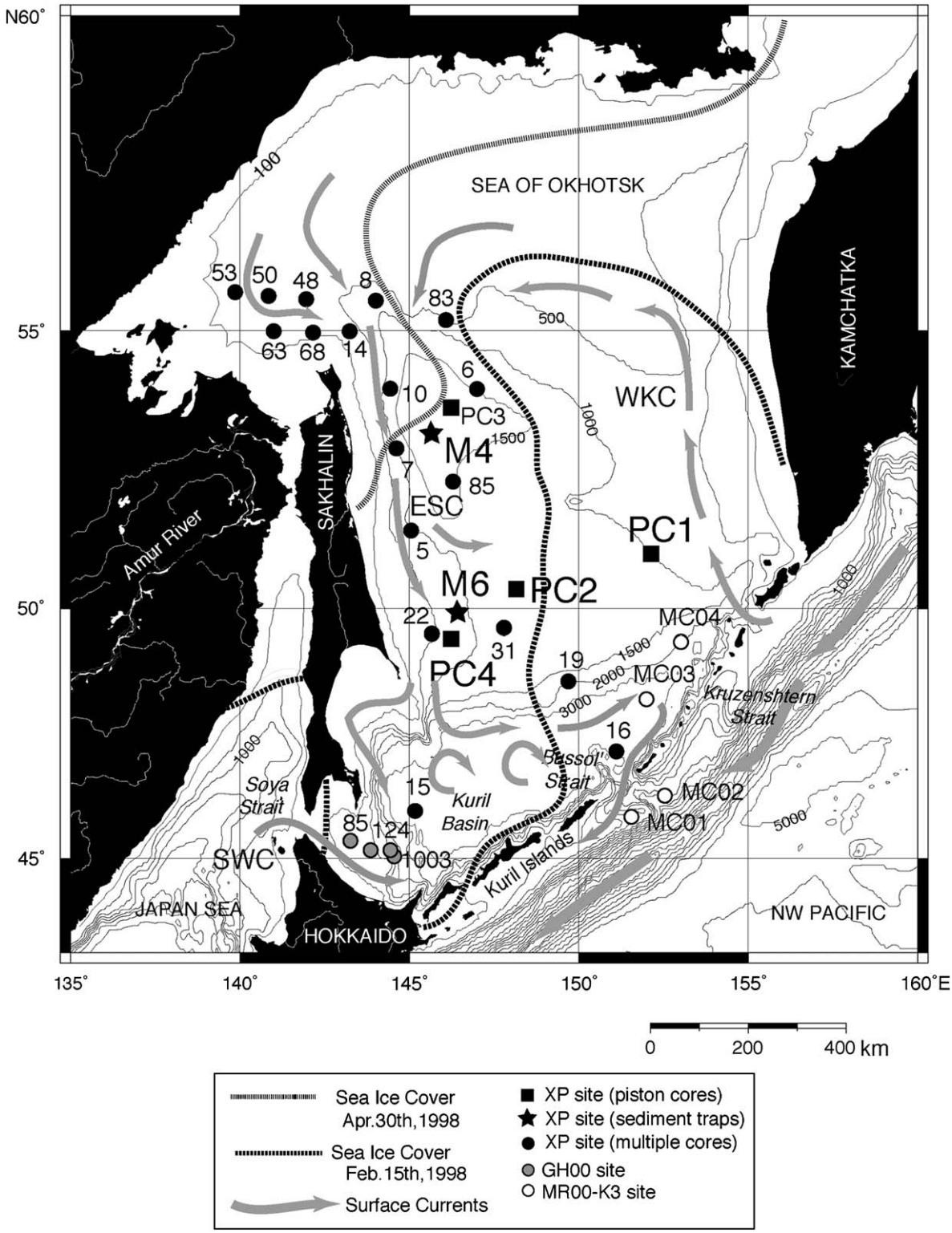

Fig. 1. Location map of the sediment traps, sea floor surficial sediments, and piston cores. Exact locations of each site are listed in Table 1. Sea floor surficial sediments were sampled during Cruises XP-98, XP-99, and XP-00 by R./V. *Professor Khromov* and Cruise MR00-K3 of JAMSTEC, and Cruise GH00 of AIST. The extent of sea-ice cover was inferred by ice charts produced by the Japan Coast Guard. WKC = the West Kamchatka Current (WKC), ESC = the Eastern Sakhalin current, SWC = the Soya Warm Current.

Table 1
Logistic information on the sediment cores obtained in the Okhotsk Sea

ID in Fig. 1	Core name	Cruise	Site	Latitude	Longitude	Depth (m)	Area	Core type	Core length (cm)	Main lithology
PC1	XP98-PC1	XP98	C1	51°00.9′N	152°00.5′E	1107	Off Kamchatka	Piston Core	1010.0	Siliceous clay
PC2	XP98-PC2	XP98	C2	50°23.7′N	148°19.4′E	1258	Academy of Sci. Rise	Piston Core	1023.0	Siliceous clay
PC3	XP98-PC3	XP98	C3	53°46.0′N	146°19.7′E	1579	Deryugin Basin	Piston Core	243.5	Siliceous clay
PC4	XP98-PC4	XP98	C4	49°29.3′N	146°07.7′E	664	Off Sakhalin	Piston Core	1128.0	Siliceous clay
16	XP99 St.16MC	XP99	16	47°12.23′N	151°06.80′E	3362	Southern Kuril Basin	Multiple cores	22.0	Siliceous clay
19	XP99 St.19MC	XP99	19	48°35.77′N	149°41.68′E	1613	Academy of Sciences Rise	Multiple cores	23.0	Siliceous clay
22	XP99 St.22MC	XP99	22	49°31.38′N	145°40.39′E	490	Off Sakhalin	Multiple cores	20.0	Silt
5	XP99 St.MC5	XP99	MC5	51°27.87′N	145°03.09′E	787	Off Sakhalin	Multiple cores	20.0	Siliceous Silt
8	XP99-MC8	XP99	C8	55°30.30′N	144°01.01′E	923	Shantarskiy Bay	Multiple cores	9.0	Sand
46	XP99 St.48MC	XP99	48	55°31.99′N	141°57.56′E	282	Shantarskiy Bay	Multiple cores	16.0	Silt
50	XP99 St.50MC	XP99	50	55°35.28′N	140°50.76′E	184	Shantarskiy Bay	Multiple cores	17.0	Silt
53	XP99 St.53MC	XP99	53	55°38.98′N	139°51.83′E	141	Shantarskiy Bay	Multiple cores	23.0	Sandy silt
63	XP99 St.63MC	XP99	63	54°59.35′N	141°00.14′E	134	Shantarskiy Bay	Multiple cores	6.0	Sand
68	XP99 St.68MC	XP99	68	54°59.28′N	141°59.80′E	117	Shantarskiy Bay	Multiple cores	6.0	Sand
83	XP99 St.83MC	XP99	83	55°08.14′N	146°01.84′E	641	Northern Deryugin Basin	Multiple cores	2.0	Sand
6	XP99-MC6	XP99	C6	53°59.84′N	146°59.81′E	1637	NE Deryugin Basin	Multiple cores	34.0	Siliceous clay
85	XP99 St.85MC	XP99	85	52°21.10′N	146°17.59′E	1440	Southern Deryugin Basin	Multiple cores	31.0	Siliceous clay
31	XP00 St.31MC	XP00	MC3	49°32.54′N	147°28.60′E	1242	Academy of Sciences Rise	Multiple cores	32.0	Siliceous clay
7	XP00 MC7	XP00	MC7	52°58.87′N	143°23.65′E	444	Northern Deryugin Basin	Multiple cores	14.0	Silty sand
14	XP00 MC14	XP00	MC14	52°00.47′N	143°00.60′E	105	Off Sakhalin	Multiple cores	8.0	Silty sand
10	XP00 MC10	XP00	MC10	51°01.89′N	142°20.28′E	1189	Northern Deryugin Basin	Multiple cores	26.0	Siliceous clay
15	XP00 MC15	XP00	MC15	46°00.29′N	144°59.42′E	3269	Western Kuril Basin	Multiple cores	26.0	Siliceous clay
85	GH00St.85	GH00	85	45°22.95′N	143°15.96′E	133	Off Hokkaido	Piston Core	23.5	Silty clay
124	GH00St.124	GH00	124	45°10.98′N	143°52.03′E	421	Off Hokkaido	Piston Core	20.0	Silty sand
1003	GH00St.1003	GH00	1003	45°03.53′N	144°33.69′E	976	Off Hokkaido	Piston Core	463.5	Siliceous silt
MC01	MR00-K3-MC-01	MR00-K3	MC01	46°18.61′N	152°32.23′E	2793	Off Kuril Islands	Piston Core	865.9	Silty sand
MC02	MR00-K3-MC-02	MR00-K3	MC02	48°15.00′N	151°59.95′E	3244	Off Kuril Islands	Piston Core	482.5	Silty sand
MC03	MR00-K3-MC-03	MR00-K3	MC03	48°15.00′N	151°59.89′E	3244	Northeastern Kuril Basin	Piston Core	461.5	Silty sand
MC04	MR00-K3-MC-04	MR00-K3	MC04	49°22.03′N	153°00.63′E	1821	Northeastern Kuril Basin	Piston Core	2060.0	Silty sand

matter in the samples was oxidized with H_2O_2 and biogenic opal in the samples was leached with Na_2CO_3. Grain-size distribution of terrigenous grains in residual samples was measured with a laser diffraction grain-size analyzer (Coulter LS230) with a repeatability of $<1\%$ about mean size. As the repeatability in the instrument depended mainly on grain dispersion and air bubbles in the sample chamber, we added small amount of sodium hexametaphosphate to the samples for dispersion and anhydrous sodium sulfite for eliminating the bubbles. The grain-size analyzer determined %volume of each size fraction with 133 detectors, ranging from 0.04 to 2000 μm in size. The grain size of some trap samples, including ones excessively large to be measured by the laser counter, was measured using an optical microscope with 2 μm precision.

Mineral assemblage of terrigenous grains was determined by Bruker AXS MXP3 X-ray diffractometer with CuKα radiation. Fine-powdered samples were set into glass-slide that have thin quantitative hallow. Each sample was analyzed at 2–40° 2θ(51.3–5.72 Å), with a step size of 0.02°. Data processing for X-ray diffractogram was performed by MacDiff software (Petschick et al., 1996).

3.4. Age model for sediment cores

Age model for piston cores was obtained by utilizing oxygen isotope ratios ($\delta\ ^{18}O$) for foraminiferal calcite, accelerator mass spectrometer (AMS) ^{14}C dates, tephra, and magnetic susceptibility (MS) (Figs. 2–4). Firstly, we present the age model for Cores XP-PC1 and XP-PC2, calculated by oxygen isotope stratigraphy, AMS ^{14}C dating, and tephra correlation (Fig. 2). Secondly, the age model of Core XP-PC4 was established by comparing the magnetic susceptibilities of Cores XP-PC2 and XP-PC4, since calcium carbonate was rare in Core XP-PC4 (Fig. 3).

Benthic foraminifer *Uvigerina auberiana ochotica* and *Uvigerina akitaensis* with test size between 212 and 355 μm were picked (>10 specimens) for the isotopic analysis. Sediment samples were washed with water and passed through a 63-μm mesh sieve, and the residual samples on the sieve were dried at 50 °C. The picked tests were cleaned with distilled water by ultrasonicator, slightly crushed in a small stainless steel cup, and reacted with 100% phosphoric acid at 60 °C in a vacuum. The released CO_2 was purified and analyzed using an isotope ratio mass spectrometer (Finnigan MAT 251) with standard NBS-20 by better than 0.03‰ analytical precision. The results are expressed by PeeDee Belemnite (PDB) standard (Fig. 2). The marine oxygen isotope stages (MIS) were recognized by graphic correlation of oxygen isotope variations of benthic foraminifer, *Uvigerina* spp., normalized to the oxygen isotope curve of Martinson et al. (1987).

Six MIS events, 3.3, 4.0, 5.0, 5.1, 5.3, and 5.51 in Core XP-PC1 and two MIS events 3.3 and 5.0 in Core XP-PC2 were identified (Fig. 2). Additional two MIS events, 3.1x and 5.1x, found in $\delta\ ^{18}O$ curve in Core XP-PC1 were correlated to Core XP-PC2. Because the upper section of Core XP-PC1 may have been lost during coring, the top is calculated to be 2.39 kyrs by comparison of $\delta\ ^{18}O$ profile of *Neoglobo-quadrina pachyderma* with that of well-dated Core V34-98 (Gorbarenko et al., 2002a, b).

AMS ^{14}C ages of planktonic foraminiferal shells *N. pachyderma* (>125 μm test size, ~10 mg in carbonate carbon) in Cores XP-PC1 and XP-PC2 were measured at the AMS facility of the Christian-Albrechts-University Kiel (Fig. 2 and Table 2). Calendar years (yr B.P.) were calculated from AMS ^{14}C ages by using a half-life of 5568 yrs, after calibration of $\delta\ ^{13}C$ using CALIB software (Stuiver et al., 1998) for ^{14}C ages younger than 24,000 cal. yrs B.P. and the calibration equation of Bard et al. (1998) for ^{14}C ages older than 24,000 cal. yrs B.P. In this calibration, we assumed that the reservoir effect of ^{14}C in the Okhotsk Sea was 950 yrs (Keigwin, 1998). All of the results of AMS ^{14}C measurement and its calibrated value were listed in Table 3.

Refractive index (RI) of glass shards and phenocrysts in each tephra were measured by thermal immersion method using RIMS-86 (RI measurement system, Kyoto Fission Track Co. at Hokkaido University) (Danhara et al., 1992) (Tables 3 and 4). Chemical composition of volcanic grass shards from 63 to 250 μm size fraction in the layers were analyzed with wavelength dispersive Electron Probe Micro-analyzer (JXA-8900 M, JEOL Co. at Hokkaido University) operated at 15 kV and using a 10 nA beam current and a 10 μm beam diameter to minimize loss of Na and K (Froggatt, 1983). Na and K are always analyzed first. Counting times of 10 s at peak are used. The compositions of the glass were calculated as a mean of 10–20 glass shards.

Four tephra layers were contained in the recovered sediment cores (Table 3): Tephra-1 (91–96 cm

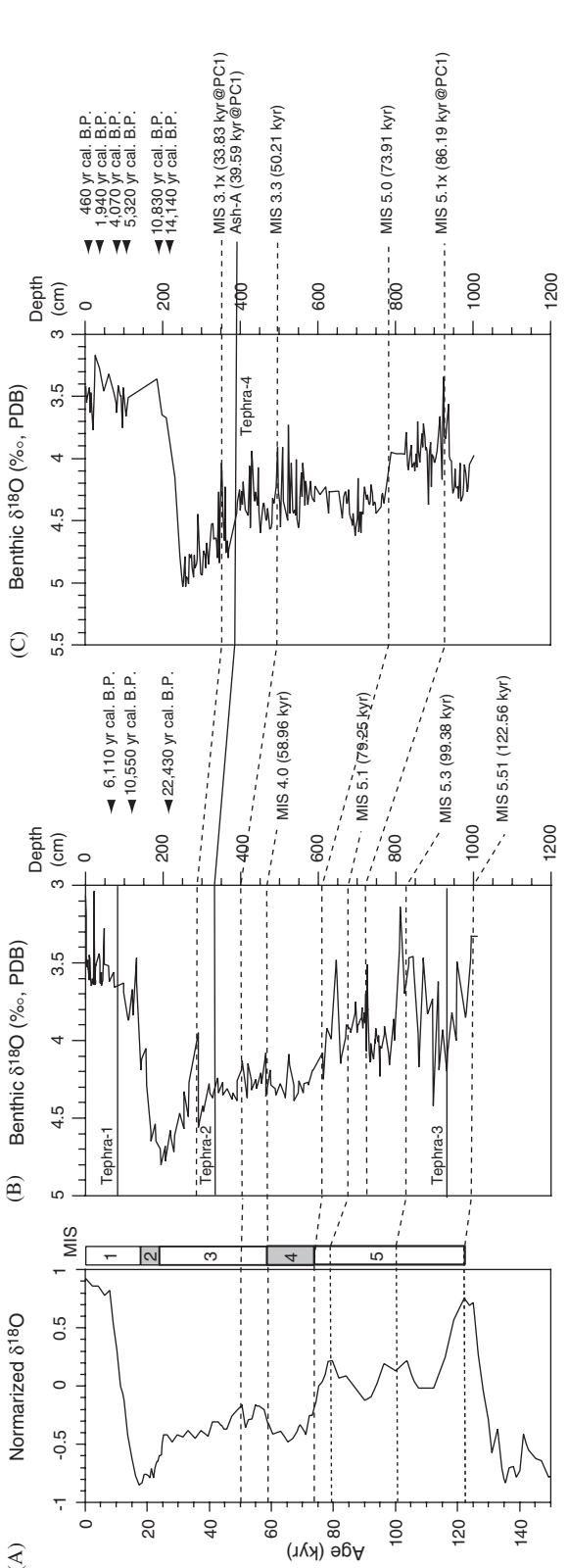

Fig. 2. Age model for piston Cores XP-PC1 and XP-PC2: (A) Normalized oxygen isotope curve of Martinson et al. (1987). (B) and (C) Oxygen isotope curves of benthic foraminifer *Uvigerina* species for Core XP-PC1 (B) and Core XP-PC2 (C). MIS = marine oxygen isotope stage. Ages shown by triangle on right side represent AMS ^{14}C dates obtained from planktonic foraminifers.

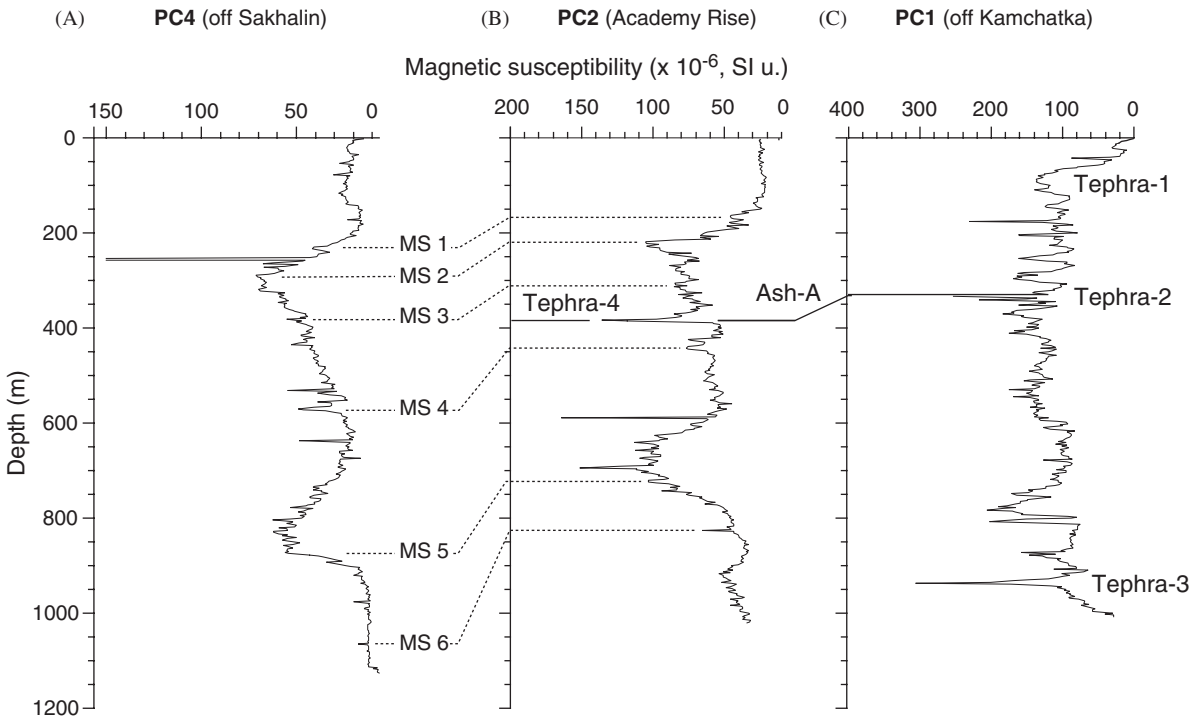

Fig. 3. Correlation among piston Cores XP-PC4 (A), XP-PC2 (B), and XP-PC1(C) by magnetic susceptibility and tephra layers. MS = magnetic susceptibility tie line.

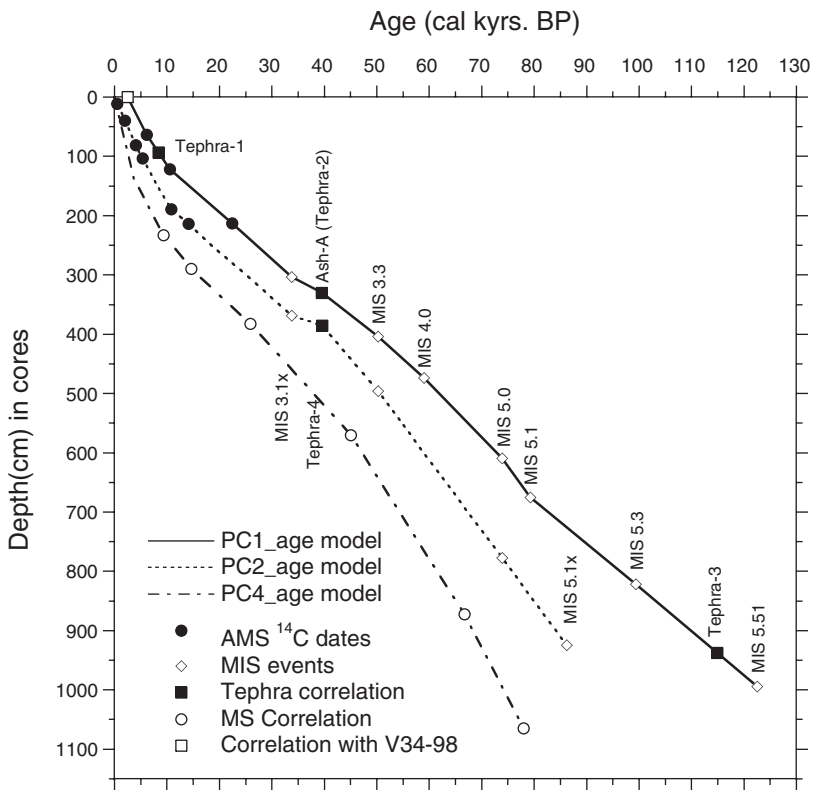

Fig. 4. Age-depth diagrams for Cores XP-PC1, XP-PC2, and XP-PC4. MIS = marine oxygen isotope stage. MS = magnetic susceptibility.

Table 2
AMS ^{14}C dates and calendar years for Cores XP-PC1 and XP-PC2

Sample ID	Depth in Core (cm)	Species	Conventional ages (yrs)	Error (yrs)	^{14}C age(years)	Calendar age (yrs)	Lab. code
PC1, 2-16	63.4	*N. pachyderma*	6245	±40	5295	6110	KIA9794
PC1, 3-1	122.2	*N. pachyderma*	10,310	±60	9360	10,550	KIA9795
PC1, 3-38	213.1	*N. pachyderma*	19,950	±130	19,000	22,430	KIA9796
PC2, 1-4˜1-6	11.1	*N. pachyderma*	1360	±25	410	460	KIA12600
PC2, 2-5˜2-7	39.5	*N. pachyderma*	2880	±30	1930	1940	KIA12604
PC2, 2-22˜2-24	81.4	*N. pachyderma*	4595	±35	3645	4070	KIA12601
PC2, 2-31˜2-33	103.6	*N. pachyderma*	5560	±35	4610	5320	KIA12603
PC2, 3-26˜3-27	189.2	*N. pachyderma*	10,570	±60	9620	10,830	KIA12599
PC2, 3-36˜3-37	214.1	*N. pachyderma*	13,250	±60	12,300	14,140	KIA12602

depth), Tephra-2 (330–331 cm depth), and Tephra-3 (934–941 cm depth) in Core XP-PC1, and Tephra-4 (383.5–388.5 cm depth) in Core XP-PC2. The measured RI of glass shards and phenocrysts and mineral assemblage in tephra layers were compiled in Table 3. Tephra-2 in Core XP-PC1 can be correlated with the Tephra-4 in Core XP-PC2, based on the RI and chemical compositions of the volcanic glass. These tephras at the different sites have almost the same values (1.506–1.509) in the RI of the volcanic glass. The similarity coefficient (Borchardt et al., 1972) of the composition between the two tephras is 0.92. It is called Ash-A in this study (Figs. 2 and 3), age of which was estimated to be 38.2–38.3 ^{14}C kyrs BP (39.5–39.6 cal. kyrs BP). Gorbarenko et al. (2002a, b) reported five widespread tephras after the last interglacial, K0 (7.7 kyrs BP), TR (8.0 kyrs BP), K2 (26 kyrs BP), K3 (60–68 kyrs BP) and K4 (100–120 kyrs BP). The age of these tephras were calculated from the age model determined by ^{14}C dating of planktonic and benthic foraminifera and the oxygen isotopic records of sediment cores. The Ash-A differs from the above five tephras in its ^{14}C dating. Most of the late Pleistocene Krakatoa-type caldera in the Kuril-Kamchatka region was established around 30–40 kyrs BP (Braitseva et al., 1995). The Ash-A would be one of the products from these volcanic activities. The age of foraminifera shells just under the Tephra-1 in Core XP-PC1 is 7.4 ^{14}C kyrs BP (8.4 cal. kyrs BP). The age of Tephra-3 in Core XP-PC1 is estimated to be 114 kyrs BP from the oxygen isotopical stratigraphy. The ages of Tephra-1 and -3 are similar to K0/TR and K4 reported in Gorbarenko et al. (2002a, b). Chemical composition of volcanic glass shards in Tephra-1 is rhyolitic and similar to K0 originated from the Kuril Lake caldera (Ponomareva et al., 2004). Similarity, coefficients are 0.90–0.94 between our data and three samples pumice fall layer samples near the Kuril Lake caldera (98KAM7.7, 98KAM7.6 and 98KAM7.5 in Ponomareva et al., 2004). Therefore, we presume that Tephra-1 in this study is correlated to K0 tephra produced by the Kuril Lake caldera-forming eruption at 7.6 ^{14}C kyrs BP in southern Kamchatka (Braitseva et al., 1995; Ponomareva et al., 2004). The information of K4 is reported only from one Core LV27-15-1 (49.0°N, 152.2°E; Gorbarenko et al., 2002a, b). The K4 is rich in gravel pumice (RI: 1.510–1.511) and volcanic glass shards (RI: 1.502–1.504), therefore Tephra-3 involving a lot of scoria and brown colored glass shards is not correlated to K4.

MS was used for correlation between cores XP-PC2 and XP-PC4. The MS is measured continuously for each cube samples (~2.5 cm intervals) of all cores using a Bartington MS-2 MS meter. The results were presented in SI units, $10^6/10\,cm^3$. The seven MS events were tied between two cores XP-PC2 and XP-PC4 with the oxygen isotope and tephra correlations (Fig. 3).

As a result, age control points for all cores were listed in Table 5. Depth-age profile was shown in Fig. 4. Liner sedimentation rate was relatively high in the eastern site (Core XP-PC1) and low in the western site (Core XP-PC4).

4. Results

4.1. Sediment traps experiments

Terrigenous flux of settling particles in the shallow traps displayed definite seasonal variations (Fig. 5). The flux was greater at Site M4 ($5.5\,mg\,m^{-2}\,d^{-1}$ on average) than at Site M6 ($4.1\,mg\,m^{-2}\,d^{-1}$), located

Table 3
Tephra layers and their refractive indices of volcanic glass and phenocrysts in sediment Cores XP-PC1 and XP-PC2 from the Okhotsk Sea

Tephra code	Core	Depth (cm)	Thickness (cm)	Estimated age (^{14}C kyrs BP)	Estimated age (cal kyrs BP)	Ash type	Mineral assemblage	Glass type	Maximum size of glass shard (μm)	Refractive index of glass (n)	Refractive index of orthopyroxene (γ)	Refractive index of hornblende (n^2)
Tephra-1	XP-PC1	91–96	5	7.4	8.4	Vitric	(opx)	pm, bw (bw*)	Fine; +125	1.503–1.505	—	—
Tephra-2	XP-PC1	330–331	1	38.2	39.5	Vitric	opx, ho	pm, bw (bw*)	Coarse; 1000	1.506–1.509	1.725–1.729	1.674–1.688
Tephra-3	XP-PC1	934–941	7	114.9	114.9	Scoria	mt (opx)	Scoria, pm*, pm	Fine; −250	1.521–1.527	—	—
Tephra-4	XP-PC2	383.5–388.5	5	38.3	39.6	Vitric	(opx)	pm, bw (bw*)	Fine; +125	1.507–1.509	—	—

opx: orthopyroxene, (opx): rare orthopyroxene, ho: hornblende, mt: magnetite, pm: pumice, bw: bubble wall type

Table 4
Chemical composition of volcanic glass in sediment Cores XP-PC1 and XP-PC2 from the Okhotsk Sea

Tephra code	Core	Depth (cm)	SiO_2 (wt%)	TiO_2 (wt%)	Al_2O_3 (wt%)	FeO^* (wt%)	MnO (wt%)	MgO (wt%)	CaO (wt%)	Na_2O (wt%)	K_2O (wt%)	n	Total (wt)%
Tephra-1	XP-PC1	91–96	77.74 (0.44)	0.21 (0.03)	12.69 (0.22)	1.55 (0.13)	0.05 (0.04)	0.20 (0.02)	1.27 (0.11)	4.18 (0.10)	2.11 (0.10)	19	96.10 (1.80)
Tephra-2	XP-PC1	330–331	76.48 (0.63)	0.27 (0.05)	12.71 (0.28)	2.25 (0.20)	0.07 (0.04)	0.22 (0.03)	1.36 (0.12)	4.11 (0.14)	2.54 (0.12)	15	95.64 (1.35)
Tephra-3	XP-PC1	934–941	—	—	—	—	—	—	—	—	—	—	—
			—	—	—	—	—	—	—	—	—	—	—
Tephra-4	XP-PC2	383.5–388.5	76.39 (0.42)	0.30 (0.04)	12.70 (0.21)	2.38 (0.13)	0.04 (0.03)	0.23 (0.03)	1.35 (0.07)	4.13 (0.10)	2.48 (0.11)	19	96.44 (1.44)

Contents of all the elements are calculated as averages (standard deviations) of 10–20 glass shards determined by electron microprobe analysis. All Fe was estimated as FeO. Chemical composition of tephra-3 in Core XP-PC-1 was not measured due to inadequate glass content for the measurement.

Table 5
Age control points for cores XP-PC1, XP-PC2 and XP-PC4

Depth (cm)	Events	Age (cal kyrs BP)	LSR (cm/kyr)	Depth (cm)	Events	Age (cal kyrs BP)	LSR (cm/kyr)	Depth (cm)	Events	Age (cal kyrs BP)	LSR (cm/kyr)
〈PC1〉				〈PC2〉				〈PC4〉			
0.0	From V34-98	2.50		0	Core top	0.00		0	Core top	0.00	
			17.6				24.1				25.0
63.4	AMS	6.11		11.1	AMS	0.46		232.9	MS1	9.31	
			13.2				19.2				10.7
122.2	AMS	10.55		39.5	AMS	1.94		289.7	MS2	14.62	
			7.6				19.7				8.3
213.1	AMS	22.43		81.4	AMS	4.07		382.8	MS3	25.89	
			7.0				17.8				9.8
332.0	Ash-A[a]	39.50		103.6	AMS	5.32		570.1	MS4	45.10	
			6.7				15.5				14.0
404.0	MIS 3.3	50.21		189.2	AMS	10.83		872.7	MS5	66.70	
			8.0				7.5				17.0
474.1	MIS 4.0	58.96		214.1	AMS	14.14		1065.0	MS6	77.98	
			9.1				7.8				
609.6	MIS 5.0	73.91		368.6	MIS 3.1x	33.83					
			12.3				3.0				
675.5	MIS 5.1	79.25		385.9	Ash-A[a]	39.59					
			7.3				10.4				
821.8	MIS 5.3	99.38		496.2	MIS 3.3x	50.21					
			7.4				11.9				
994.3	MIS 5.51	122.56		777.3	MIS 5.0	73.91					
							12.0				
				924.6	MIS 5.1x	86.19					

AMS = ^{14}C ages determined by the accelerator mass spectrometer methods, MIS = marine oxygen isotope stage events, MS = correlation by magnetic susceptibility, and LSR = linear sedimentation rate

[a]Age of Ash-A was calculated age in this study.

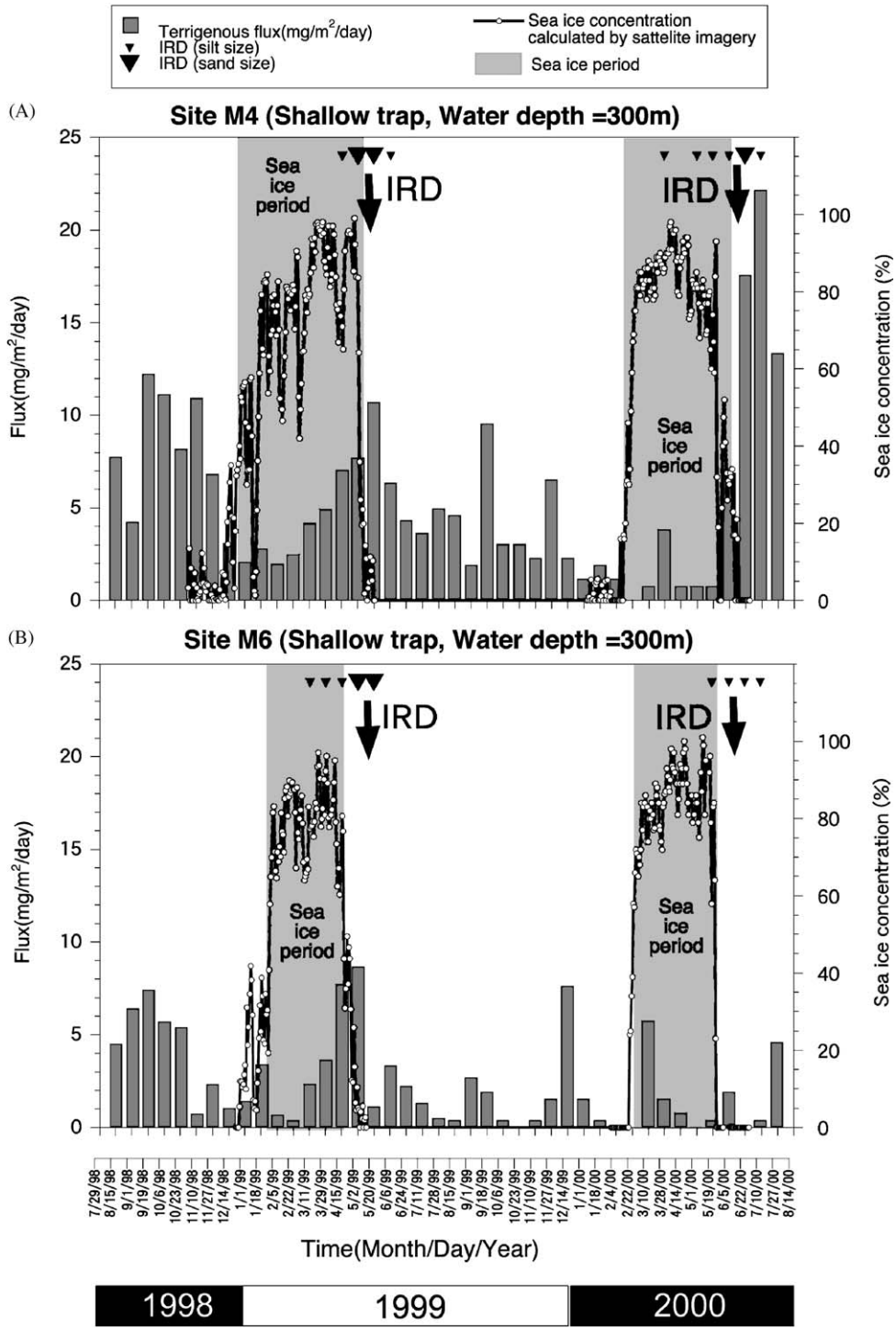

Fig. 5. The variations of terrigenous flux in sediment trap experiments: (A) Site M4, (B) Site M6. Four time-series sediment traps were positioned at Sites M4 and M6 located off Sakhalin Island from August 1998 to July 2000. Results are from the upper traps (300 m water depth) at both sites. Each bar indicates the total terrigenous flux in each cup, as measured by organic-free residual weight. The triangle shows the location of large and small angular terrigenous grains observed in filtered trap samples under a stereoscope. Sea-ice concentration curves were calculated by a modified NASA algorithm (Kimura and Wakatsuchi, 1999) from the brightness temperature of DMSP SSM/I.

250 km south from Site M4. The flux at Site M4 generally showed maxima in autumn, 12.2 mg $m^{-2} d^{-1}$ in 1998 and 9.5 mg $m^{-2} d^{-1}$ in 1999, and spring, 10.7 mg $m^{-2} d^{-1}$ in 1999 and 22.1 mg $m^{-2} d^{-1}$ in 2000. The flux at Site M6 increased in autumn 1998 (7.4 mg $m^{-2} d^{-1}$) and in spring 1999 (8.7 mg $m^{-2} d^{-1}$) and frequently increased in several times from 1999 autumn to 2000 spring.

Sea-ice concentration which was calculated by satellite imagery, gradually increased from the middle November to the late April 1999 and retreated quickly in May at Site M4. Sea-ice cover at Site M6 appeared two month later than Site M4 and disappeared earlier than Site M4 in 1999. Corresponding to these sea-ice extents, the terrigenous flux gradually increased during the sea-ice formation in 1999 winter, peaked just after melting of sea-ice at both sites in 1999 spring, and decreased gradually. The peak of 1999 spring flux at Site M4 was delayed by two weeks, in comparison with Site M6, since sea-ice prevailed longer at this site. Sea-ice in 2000 winter at both sites covered and retreated very quickly compared to the 1999 winter. The extreme peak in spring 2000, with sand-sized particles, was found only at Site M4, whereas a few silt-sized settling particles were found at Site M6. Because satellite imagery showed that sea-ice suddenly (within 2 weeks) retreated from the location of Site M6 to the north and melted at around Site M4 in June 2000, the spring fluxes were obviously related to the extent of sea-ice cover.

As noticeable results, sand-sized and silt-sized angular terrigenous grains were observed under a stereoscope on filtered sediment trap samples during the melting of sea-ice in spring (Figs. 5 and 6), although we were able to identify the grains only qualitatively because of the availability of a very small amount ($<$ 0.05 g in average) of samples.

Based on the detailed analyses for terrigenous flux at Sites M4 and M6 from August 7, 1998 to 1999, we were able to show the modern process of IRD sedimentation in the western side of the Okhotsk Sea. Total terrigenous flux at Sites M4 increased earlier than at Site M6 in February 1999 and reached a maximum following that of Site M6 in early May 1999 (Fig. 6A). There are two peaks of the flux in autumn and spring in 1999. The contents of the two peaks are clearly different, which are identified by visible domain, diffuse-color reflectance measurements, grain-size analyses, and microscopic observation of filtered trap samples at Sites M4 and M6. The flux material during spring 1999 showed relatively light-colored surfaces on the filtered samples and consisted mainly of angular silt- and sand-sized particles, with clay-sized particles being subordinate (Figs. 6B, D, and F). Sand- and silt-sized angular terrigenous grains, which were mainly composed of quartz and feldspar, were observed during the melting of sea-ice in spring 1999 (Fig. 6A). The amount of spring terrigenous flux mostly represented the amount of IRD flux. In contrast, the autumn flux appeared darker in color than the spring flux, consisting mainly of clay- and silt- sized particles, with rare sand-sized particles (Figs. 6B, C, and E). In addition, grain-size distribution of autumn and spring flux was consistent with those of the interglacial and glacial samples in sediment cores (Figs. 6G and H).

4.2. Sea floor surficial sediments

Horizontal distribution of the relative abundance of large terrigenous particles (63–2000 μm in diameter) of surficial sediments is positively correlated with the mean sea-ice extent during the winter (Fig. 7A). The coarser particles were abundant in surficial sediments of the northern and western region ($>$5%), and less in the eastern open ocean conditions ($<$1%). The differences were mainly attributed to sea-ice coverage. We suggest that surficial sediments including greater than 5% volume terrigenous grains, indicate regions, which were covered by seasonal sea-ice every winter. Very high percentages ($>$80%) of large size terrigenous particles can be associated with coastal sedimentary environments around the Hokkaido and the Kuril islands.

Mineral assemblages of terrigenous grains in the surficial sediments also correlate with grain size, and hence, mean sea-ice extent. The sediments in the northern and western side of the Okhotsk Sea are relatively predominated by feldspar (Fig. 7B). Sediments located near the Kamchatka Peninsula and the Kuril Islands are rich in hornblende, reflecting volcanic and volcaniclastic rocks which crop out (Fig. 7C) in these regions.

4.3. Grain-size distribution and mineral assemblages of terrigenous flux in piston cores

All grain-size distribution of terrigenous particles in Cores XP-PC1, XP-PC2, and XP-PC4 are plotted in Fig. 8. It is clearly observed that there is not so

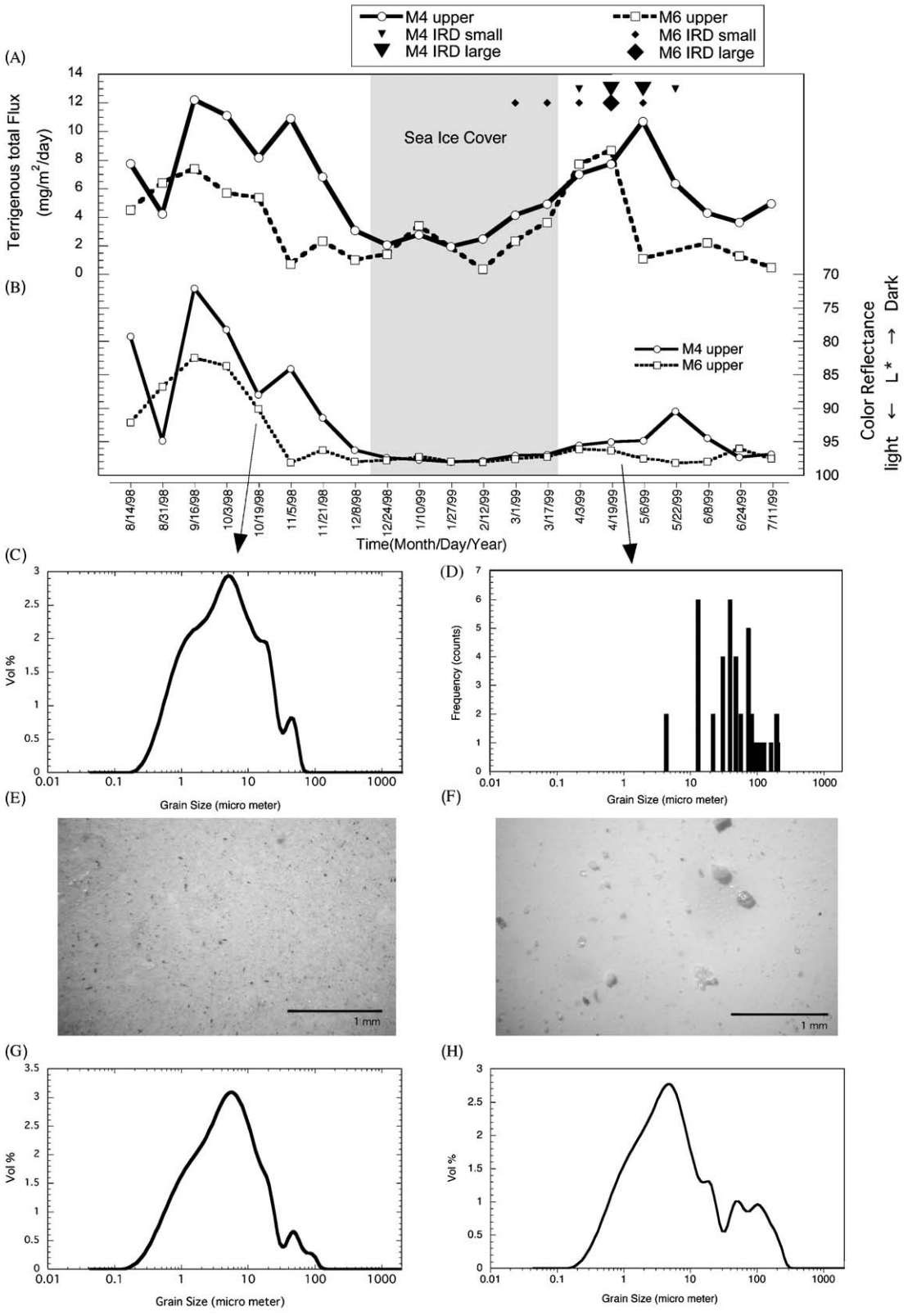
(A)
M4 upper
M6 upper
M4 IRD small
M6 IRD small
M4 IRD large
M6 IRD large
Terrigenous total Flux (mg/m2/day)
Sea Ice Cover
(B)
M4 upper
M6 upper
Color Reflectance
light ← L* → Dark
8/14/98
8/31/98
9/16/98
10/3/98
10/19/98
11/5/98
11/21/98
12/8/98
12/24/98
1/10/99
1/27/99
2/12/99
3/1/99
3/17/99
4/3/99
4/19/99
5/6/99
5/22/99
6/8/99
6/24/99
7/11/99
Time(Month/Day/Year)
(C)
Vol %
Grain Size (micro meter)
(D)
Frequency (counts)
Grain Size (micro meter)
(E)
1 mm
(F)
1 mm
(G)
Vol %
Grain Size (micro meter)
(H)
Vol %
Grain Size (micro meter)

much of variation in clay- and silt-sized fractions, but a substantial variation is seen in sand-sized fraction (Figs. 8A–C). The distribution can be classified into two types (Fig. 8D). Type-A has a bimodal distribution with maxima around 5 and 200 μm in diameter, which is often found with dropstones in the glacial samples. Type-B has a unimodal distribution rich in clay- and silt-sized terrigenous grains with only a minor amount of sand-sized fraction. This type is usually found in the interglacial samples.

Quartz, feldspars, and clay minerals dominate the terrigenous fraction, with hornblende and augerine-augite predominating in the 63-μm heavy fractions. In terms of spatial distribution, feldspars were relatively enriched in the western part of the Okhotsk Sea, decreasing to the east (Fig. 9A). In turn, hornblende was particularly abundant at the eastern location, around Core XP-PC1 (Fig. 9B), and is consistent with the sea floor sediment mineral assemblages (Fig. 7).

4.4. Definition and calculation of IRD fraction

IRD fraction in the Okhotsk Sea was defined as >63 μm terrigenous particles based on sample observations of sediment traps, surficial sediments, and sediment cores. Sediment trap experiments revealed that the amount of spring terrigenous flux mostly represented the amount of IRD flux. The amount of terrigenous fraction of 63–2000 μm in surficial sediments corresponds to seasonal sea-ice coverage. The coarser fraction (63–2000 μm) of the bimodal grain-size distribution (Type-A) in sediment cores is IRD.

The IRD content for each sample was calculated as a volume fraction of the particles ranging from 63 to 2000 μm in total fraction. The fraction of >2000 μm (dropstones) was not included in IRD calculation because the small amount of large particles can only be used for qualitative estimation of IRD fraction but not for inclusion for the quantitative estimation by the laser diffraction grain-size analyzer. As a reference, a total of 61 dropstones were collected in Cores XP-PC1 (8 stones), XP-PC2 (23 stones), and XP-PC4 (30 stones). Those are mainly of sub-angular and sub-rounded shape. The mean size of the dropstones is 16.83 mm, with a range of 2.35–66.35 mm. Their mean sizes among cores are not substantially different: 13.48, 19.83, and 17.18 mm in Cores XP-PC1, XP-PC2, and XP-PC4, respectively.

4.5. IRD variations in piston cores

The content of IRD varied on the glacial–interglacial scales (Fig. 10). IRD content increased during the glacial periods (MIS2 and 4) at all locations. The glacial peaks of IRD in the western part (Core XP-PC4) were broader than that in the eastern part (Core XP-PC1). IRD was always found in the western part of the Okhotsk Sea during the last 80 kyrs. In the central part (Core XP-PC2), IRD clearly increased during the glacial stages. IRD content in the eastern part was relatively low except for occasional and abrupt peaks. Minima in IRD appeared during the warm periods around 82, 48 kyrs, and the present. Almost no IRD has been recorded in the central part during the past 9 kyrs.

Short-term, millennium-scale variations of IRD were superimposed on the glacial–interglacial cycle. Most of those appeared as sudden and abrupt peaks of greater than 10% volume IRD. The amplitude of the variations was enhanced especially during the cold periods. The abrupt IRD peaks appeared more frequently in the western part (Core XP-PC4) and are absent in the eastern part around MIS4. The high-frequency variation in the western part began prior to 82 ka and terminated at about 48 ka. Feldspars are common in IRD variations in the western part (Fig. 9). The abrupt accumulation of IRD resumed at about 40 ka

Fig. 6. Detailed variations of terrigenous flux in sediment trap experiments from 7 August 1998 to 1999: (A) Total terrigenous flux at Sites M4 and M6. The triangle and diamonds show the locations of large (sand-size) and small (silt-size) angular terrigenous grains observed in filtered trap samples under the stereoscope. (B) Visible domain, diffuse-color reflectance of filtered trap samples at Sites M4 and M6. The autumn flux appears darker in color than the spring flux. (C) Grain-size distribution of autumn flux by laser grain-size analyzer (Sample from Trap No. 5 at Site M4). (D) Grain-size distribution of spring flux by digital-image processing (Sample from Trap No. 16 at Site M6). (E) Digital image of the autumn flux. (F) Digital image of the spring flux. (G) Grain-size distribution of the interglacial periods by laser grain-size analyzer (Sample from sediment Core XP-PC4, Section 2, 84.9 cm depth (No. 21), 2 kyrs cal. BP). (H) Grain-size distribution of the glacial periods by laser grain-size analyzer (Sample from sediment Core XP-PC4, Section 5, 341 cm depth (No. 7), 18.9 kyrs cal. BP).

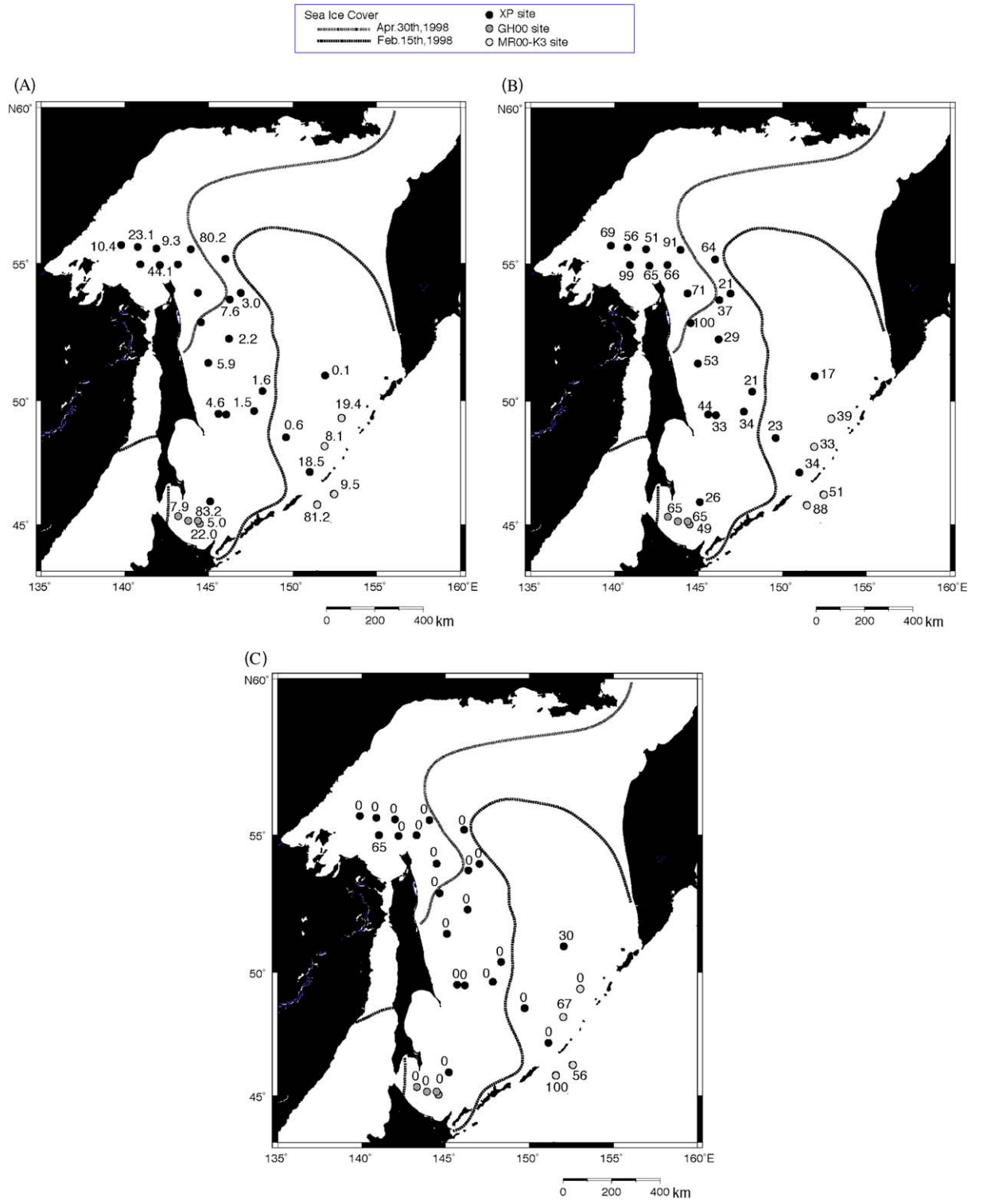

Fig. 7. Lateral distribution of grain size and minerals of terrigenous grains within the sea floor surficial sediments: (A) Lateral distribution of coarse fraction of terrigenous grains. Coarse fraction is defined as a grain size greater than 63-μm. Numbers at all site locations represent %volume of coarse fraction in the sediments. (B) Lateral distribution of feldspar content in terrigenous grains. Numbers at all site locations mean relative intensity of X-ray diffraction in the sediments. (C) Lateral distribution of hornblende content in terrigenous grains. The numbers at all site locations represent relative intensity of X-ray diffraction in the sediments.

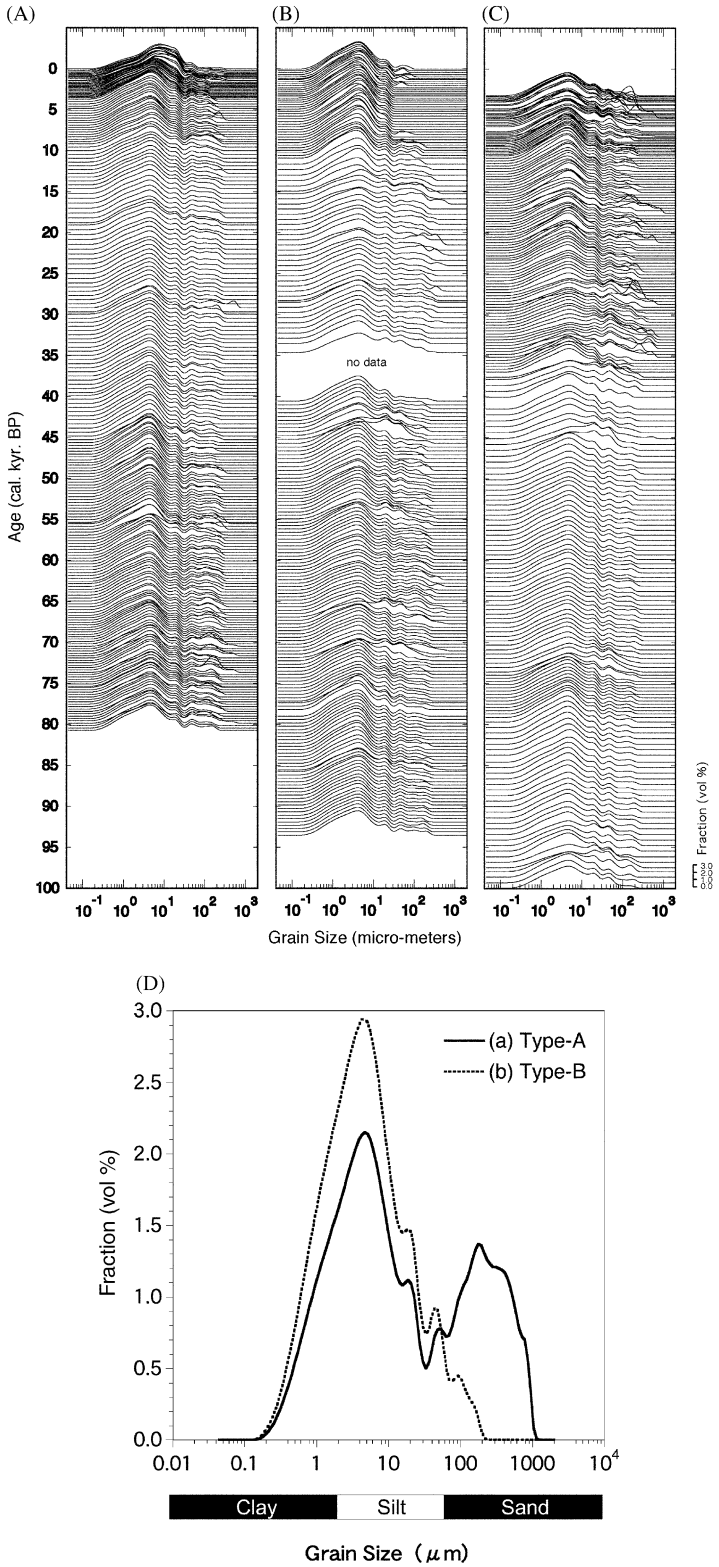

Fig. 8. Results of grain-size analysis for (A) Cores XP-PC4, (B) XP-PC2, (C) XP-PC1, and (D) typical grain-size distribution of terrigenous grains from piston cores from the Okhotsk Sea . (i) Type-A: Sample from piston Core XP98-PC1, Section 3, No. 23U (Glacial interval). (ii) Type-B: Sample from piston Core XP98-PC1, Section 1, No. 8U (Interglacial interval).

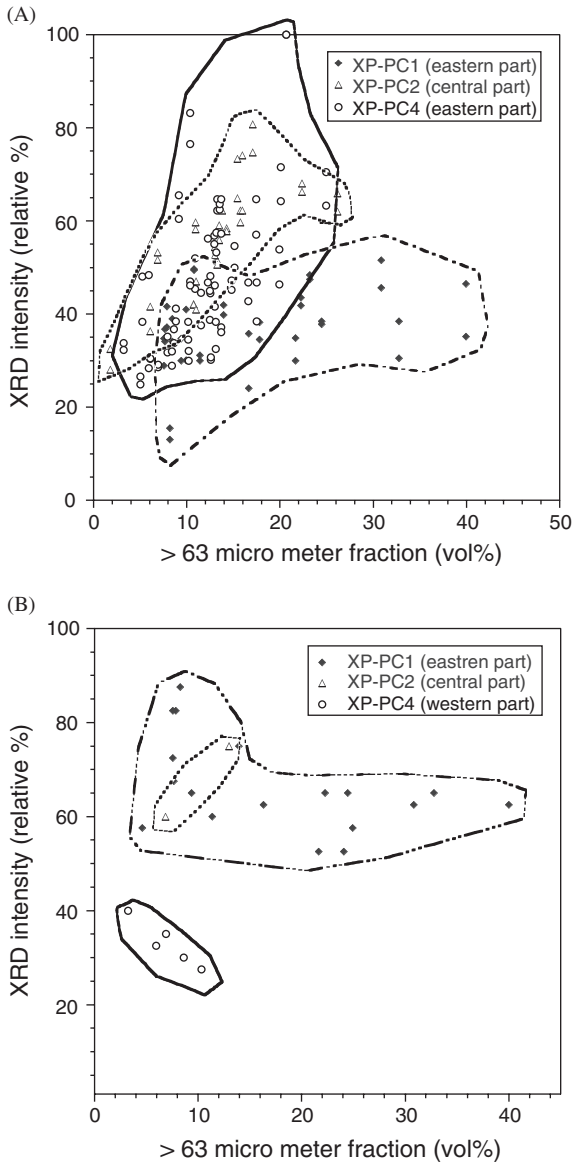

Fig. 9. Relative contents of feldspar (A) and hornblende (B) in piston Cores XP-PC1, XP-PC2, and XP-PC4. XRD intensity is calculated from the peak intensity of the mineral versus maximum intensity of the mineral in the analyses.

over the entire Okhotsk Sea. The maximum amplitude, greater than 20%, appeared during the last glacial stage (MIS2) in the central and the eastern areas. The maximum observed in the eastern area during the interglacial stages before and after MIS2 were not found in the central and western areas. Those abrupt accumulations of IRD in the eastern area were particularly abundant in hornblende (Fig. 9).

5. Discussion

5.1. Origins of IRD

The origins of IRD can be constrained from mineral assemblages in the surficial sediments and piston cores combined with the present distribution of sea-ice. Feldspars are a major mineral of IRD components in most surficial sediments of the northern and western part of the Okhotsk Sea (Figs. 7 and 9). Amount of feldspar is interpreted to reflect the extent of sea-ice. Feldspars in IRD from sediment cores have been enriched in the western part of the Okhotsk throughout the past 100 kyrs. Based on the analogy from satellite imagery that most sea-ice originates from the northern part of the Okhotsk Sea and expands into the central and eastern parts, the IRD during the past 100 kyrs must have mainly derived from the northern and western continental margin.

Distinct peaks of IRD appeared during the last ~40 kyrs, which are observed only in Core XP-PC1 off Kamchatka. Not only volcanic origin grains such as pumiceous fragments and volcanic glass but also sub-rounded siliciclastic mineral grains are included in the peaks, which are relatively richer in hornblende than in other cores. The source of IRD fraction in the eastern part of the Okhotsk Sea during ~40 kyrs is regarded to be related siliciclastic and volcanic deposits on the Kamchatka Peninsula and/or the Kuril Islands.

The simplest interpretation of the distinct peaks of IRD data would be that there were icebergs rafted from the advanced glacier on the western Kamchatka Peninsula in the Pleistocene. Today, mountain glaciers exist on the Kamchatka Peninsula, being on the average 1500 m above the sea level (World Glacier Inventory, National Snow and Ice Data Center, University Colorado, USA). A study of glacial moraines in this region (Savoskul, 1999) indicates that the glaciers have been advanced in several times even during the Holocene. The mountain glaciers could have largely extended during the glacial times. Although the present glaciers all drain into the east of the Kamchatka Peninsula today, it needs more consideration: whether or not the glaciers have reached on western coastal area of the peninsula and released icebergs to the sea during the glacial period. This is because a good number of glacial troughs on the alluvial plains are easily found on a topographical map in the western flank of the

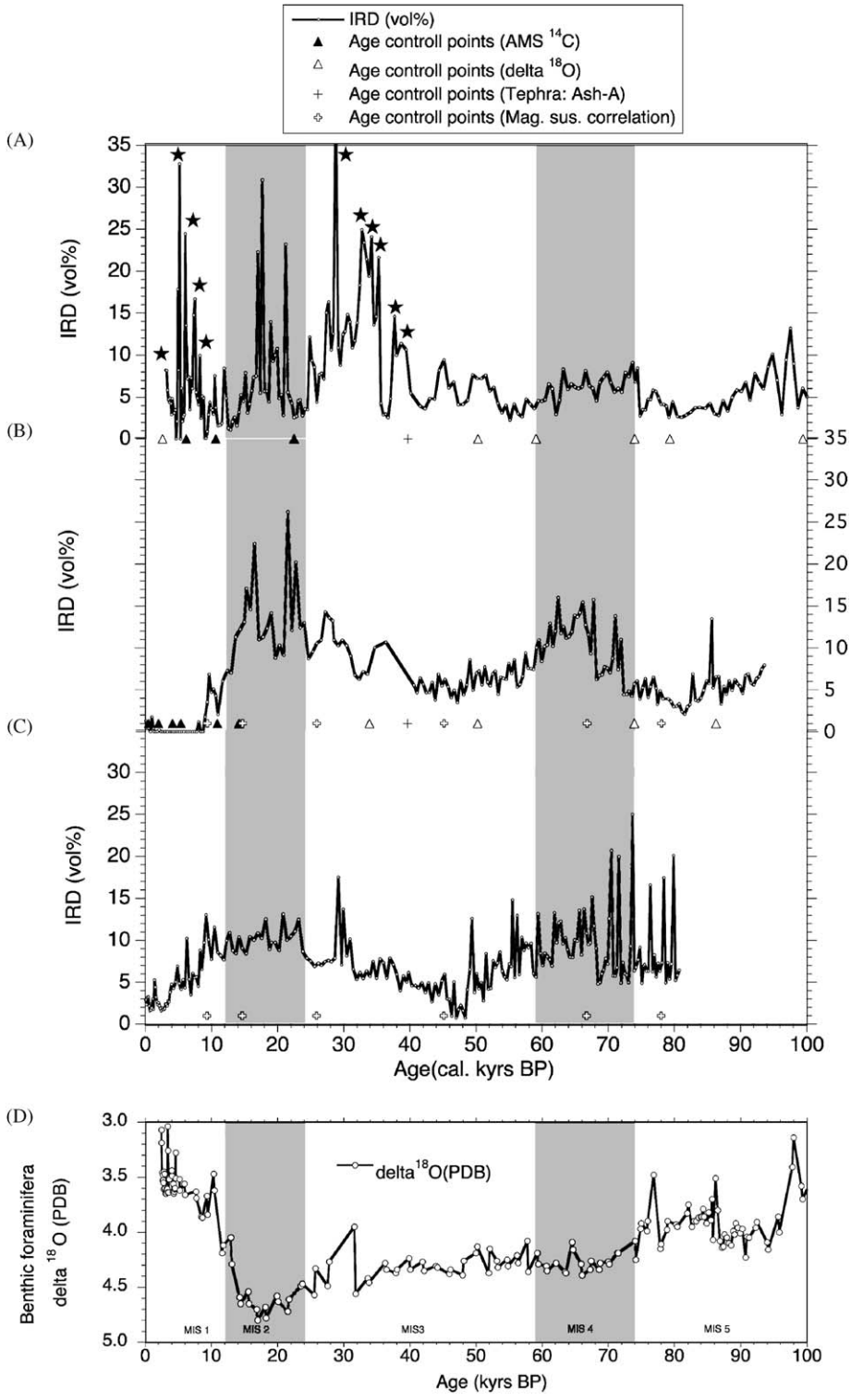

Fig. 10. IRD variations of Cores XP-PC1 (A), XP-PC2 (B), and XP-PC4 (C) in the Okhotsk Sea during the past 100 kyrs with the oxygen isotope variation of benthic foraminifers in Core XP-PC1. Time control-points in the figure are listed in Table 2. The stars in (A) shows unique peaks including hornblende found only at Site XP-PC1. MIS = marine oxygen isotope stage.

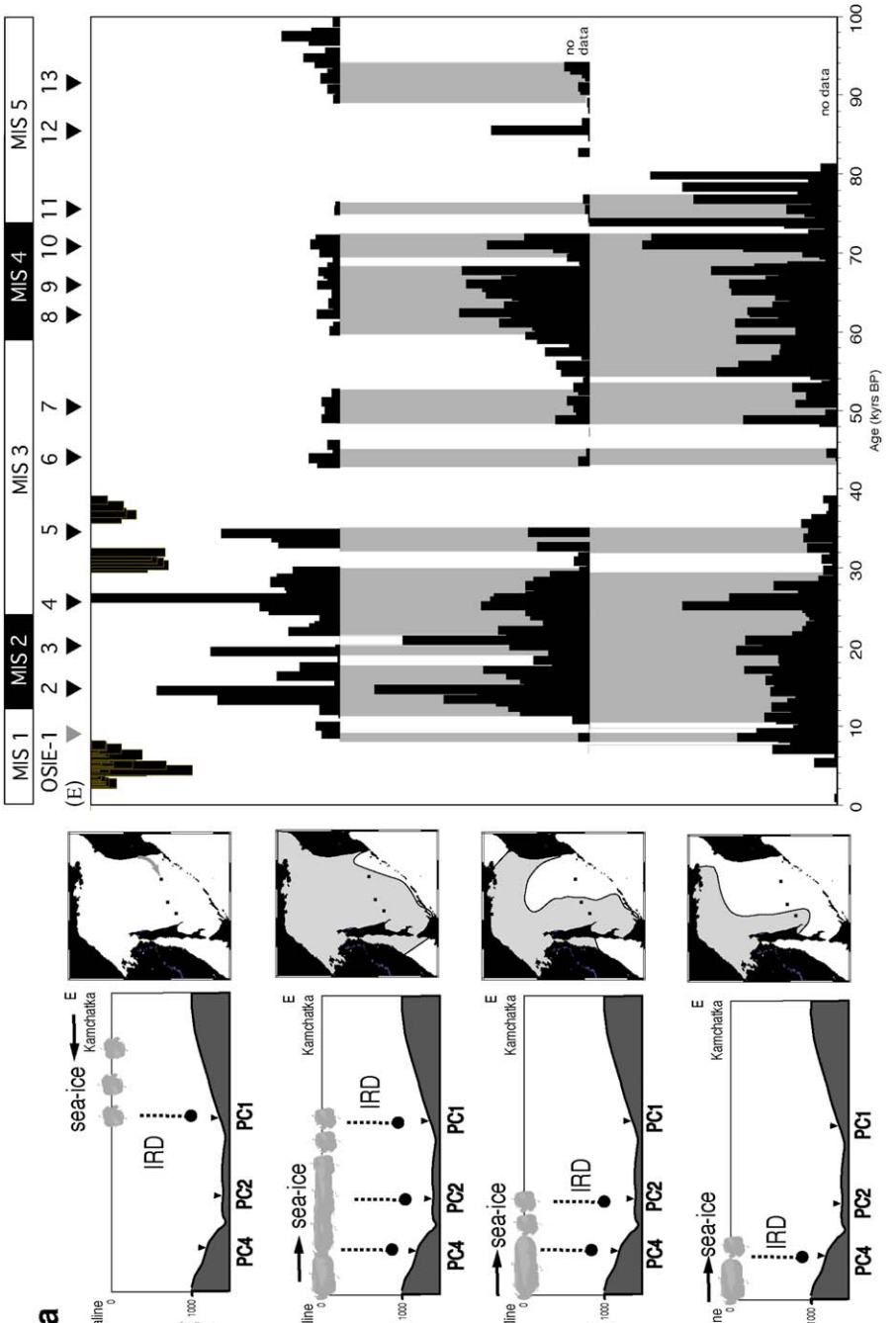

Fig. 11. Reconstruction of sea-ice expansion during the past 100 kyrs in the Okhotsk Sea. Sea-ice expansion is divided into the four intervals. Bathymetry is contoured with core locations along the East–West transect. Sea-ice expansions for each of the interval are substantiated by analogy with present day satellite observations: (A) Mode Extra: only the interval in which abrupt peaks of IRD are recognized in Core XP-PC-1 where sea-ice was derived from the regions around the Kamchatka Peninsula. (B) Mode I: the interval of maximum sea-ice expansion, which is defined by the appearance of IRD in every Cores XP-PC1, XP-PC2, and XP-PC4. (C) Mode II: the interval of moderate sea-ice expansion, which is defined by the appearance of IRD in Cores XP-PC1 and XP-PC2. (D) Mode III: the interval of minimum sea-ice expansion, which is defined by the appearance of IRD only in Core XP-PC1. (E) Spatial and temporal series reconstruction of sea-ice expansions during the past 100 kyrs. Black-shaded area represents $>5\%$ IRD contents in each of the samples. Gray-shaded area represents correspondent IRD peaks among cores, representing spatial and temporal serial reconstruction of sea-ice expansion. In the case where IRD peaks are recognized in all cores, gray area represents that sea-ice expanded from the location of Core XP-PC4 to that of Core XP-PC1 (i.e. Mode I). Dark-shaded area in the upper part in (E) represents IRD peaks recognized only in Core XP-PC1. The triangles with numbers indicate the OSIE. MIS = marine oxygen isotope stage.

Kamchatka Peninsula. Increased terrigenous flux during the glacial times in the eastern part of the Okhotsk Sea can be interpreted as evidence of iceberg release. If the glaciers did not reach to sea level on the western side of the peninsula, as mentioned by Frenzel et al. (1992), another possible transportation of terrigenous coarse grains would be coarse grains that were caught into sea-ice during grounding near the coastline on continental shelf off Kamchatka and/or the Kuril Islands. The grains are unlikely to be transported directly by eolian fallout of volcanic eruption because that the grains are sub-round or sub-angular shape and poorly sorted.

5.2. IRD as a proxy for reconstruction of sea-ice expansion

Before using IRD as a proxy for past sea-ice expansion, a paleoceanographic regime shown by the proxy must be proposed. The development of the Aleutian Low results in a strong wind field, creating a colder climate over the Okhotsk region expanding the sea-ice cover in the Okhotsk Sea (Kimura and Wakatsuchi, 1999). The southerly wind transports sea-ice toward south, which is formed in the northern part of the sea, creating a polynya along the coast resulting the formation of new sea-ice. The increase in the settling flux of terrigenous grains during spring is caused by the lateral retreat of sea-ice, as be observed by satellite imagery. Sea-ice concentration, which can be calculated from satellite images, indicates that sea-ice forms earlier and disappears later at Site M4 than at Site M6, accounts for the 2-week-phase lag in sediment flux between these sites. The low terrigenous flux at Site M4 during winter 2000 was caused by the duration of high concentration of sea-ice. Sea-ice melting and retreat, from south to north during early spring 2000, resulted the extreme peaks of terrigenous flux in 2000, which were only recorded at Site M4. The results of the sediment trap study indicate that the spring flux, consisting of silt- and sand-sized terrigenous grains, was IRD that sank after sea-ice melting. On the other hand, the fall terrigenous flux presumable was not IRD since there is no sea-ice there. The fall flux is attributed to the grain transport by the cold and dense East Sakhalin Current that becomes strong during fall and winter.

The grain-size distributions observed in the piston cores were consistent with the autumn and spring sediment trap experiments (Fig. 6). Therefore, the two dominant grain-size distribution patterns observed within the piston cores, most likely formed by long-term integration of annual fluxes including both the spring and autumn fluxes. The bimodal distributions of Type-A patterns are integrated products of autumn sedimentation with spring IRD deposition, whereas Type-B distributions are the result from interglacial with low extent of sea-ice conditions.

The presence of IRD in all cores, even at Site XP-PC1, which is currently ice-free (Fig. 10), indicates that during colder periods, sea-ice must have expanded to cover all of the Okhotsk Sea. Short-term IRD variations were significantly enhanced in amplitude during periods when global ice sheets expanded. The increase in IRD content of the cores is directly related to the expansions of sea-ice under colder climatic conditions. Under these cold conditions and strong wind fields, sea-ice expanded rapidly, and with lowered sea level and exposed greater expanse of continental shelf, the capturing and transport of terrigenous grains was enhanced.

Even during the glacial periods, sea-ice cover in the Okhotsk Sea could not have been perennial, but rather seasonal and/or over-annual melting occurred with the release and deposition of IRD. Okazaki et al. (2003) also reported that sea-ice cover during the glacial in the Okhotsk Sea would be seasonal condition based on radiolarian assemblages. Based on diatom analyses Gorbarenko et al. (2003) mentioned that summer ice melting and delivery of a significant amount of ice-rafted material during the glaciation in major part of

Table 6
Estimated age of the Okhotsk Sea-ice expands events (OSIE)

Events	Age (kyrs cal. BP)	Age (kyrs BP)
OSIE-1	9.3–10.3	8.2–9.1
OSIE-2	15.3–16.5	13.4–14.6
OSIE-3	21.5–22.7	19.6–20.8
OSIE-4	27.2–28.3	25.2–26.3
OSIE-5	34.6–36.3	32.7–34.6
OSIE-6	44.2–45.7	43.5–45.1
OSIE-7	49.0–51.3	48.9–51.3
OSIE-8	62.0–62.4	62.0–62.4
OSIE-9	64.8–67.7	64.8–67.7
OSIE-10	71.0–71.9	71.0–71.9
OSIE-11	75.1–75.5	75.1–75.5
OSIE-12	85.6–85.6	85.6–85.6
OSIE-13	93.1–93.5	93.1–93.5

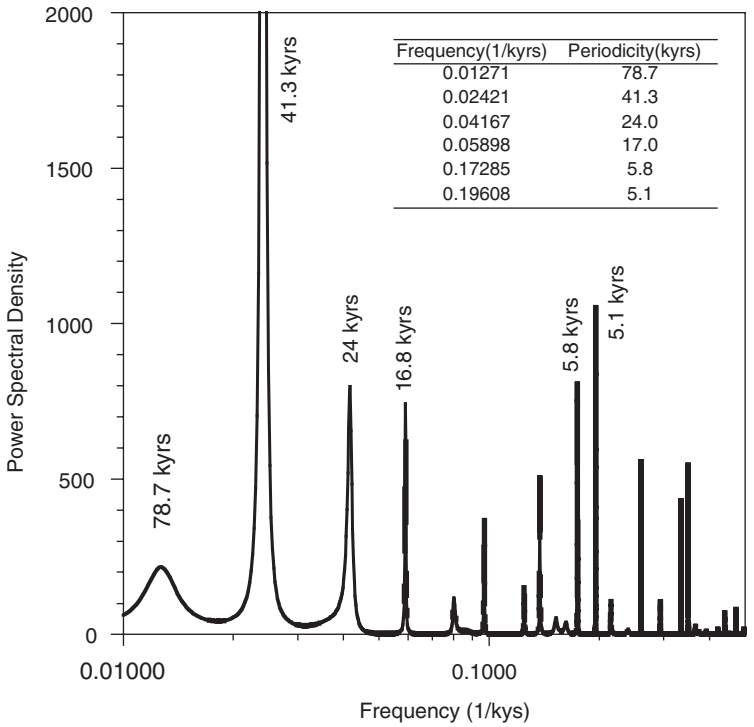

Fig. 12. Spectral analysis of IRD variation of Core XP-PC2. Spectra are obtained by maximum entropy methods (MEM). Total number of data is 206 points. Average sampling interval (Δt) is calculated to be 0.45 kyrs. Nyquist frequency ($1/2\Delta t$) is 0.23.

Okhotsk Sea by ice-rafted material. They also mentioned that only the northwestern most part of the sea was covered by year-round sea-ice during the glaciation. Diatom assemblages reported by Shiga and Koizumi (2000) also suggest that perennial sea-ice conditions were unlikely in most of the Okhotsk Sea.

5.3. *Reconstruction of sea-ice history in the Okhotsk Sea*

Sea-ice expansion in the Okhotsk Sea during the past 100 kyrs can be reconstructed by IRD variations (Fig. 11). Comparable IRD peaks are observed in all Cores XP-PC1, XP-PC2 and XP-PC4 without intersection of time control points. The well-dated Core XP-PC1 is used to correlate IRD peaks among cores.

Past sea-ice conditions can be categorized into the following four conditions (Figs. 11A–D); Mode I: the state of maximum sea-ice expansion, defined by the appearance of IRD in all cores. Mode II: state of moderate sea-ice expansion, defined by the appearance of IRD in Cores XP-PC1 and XP-PC2. Mode III: state of minimum sea-ice expansion, defined by the appearance of IRD only in Core XP-PC1. Mode Extra: Some abrupt peaks are only recognized within Core XP-PC-1 where IRD may have been derived from around the Kamchatka and/or Kuril islands.

Fig. 13. Correlation between Greenland ice core records and IRD variations in the Okhotsk Sea at Site XP-PC 2: (A) Stable isotope ($\delta\,^{18}O$) data from GRIP and GISP2 ice cores (White et al., 1997; Stuiver et al., 1995; Steig et al., 1994). The Heinrich events above the isotopic curve are from Bond et al. (1993). (B) Band-pass components of the PCI calculated by Mayewski et al. (1997), which contain greater than 70, 36.5, and 6.3-kyr components. (C) PCI calculated by Mayewski et al. (1997). An increase in PCI indicates colder polar environments. (D) Heinrich events in marine sediment core DSDP Site 609 in the Northern Atlantic (Bond et al., 1992). (E) The OSIE in the central part (Site XP-PC2). (F) IRD variation at Site XP-PC2. (G) Band-pass components of IRD variation at Site XP-PC2, which contains 78.7, 41.3, 24.0, and 5.1-kyr periodicities. Age scale of this study (E–G) is independent of GRIP and GISP2 ice cores (A–C) and of the Heinrich events (D).

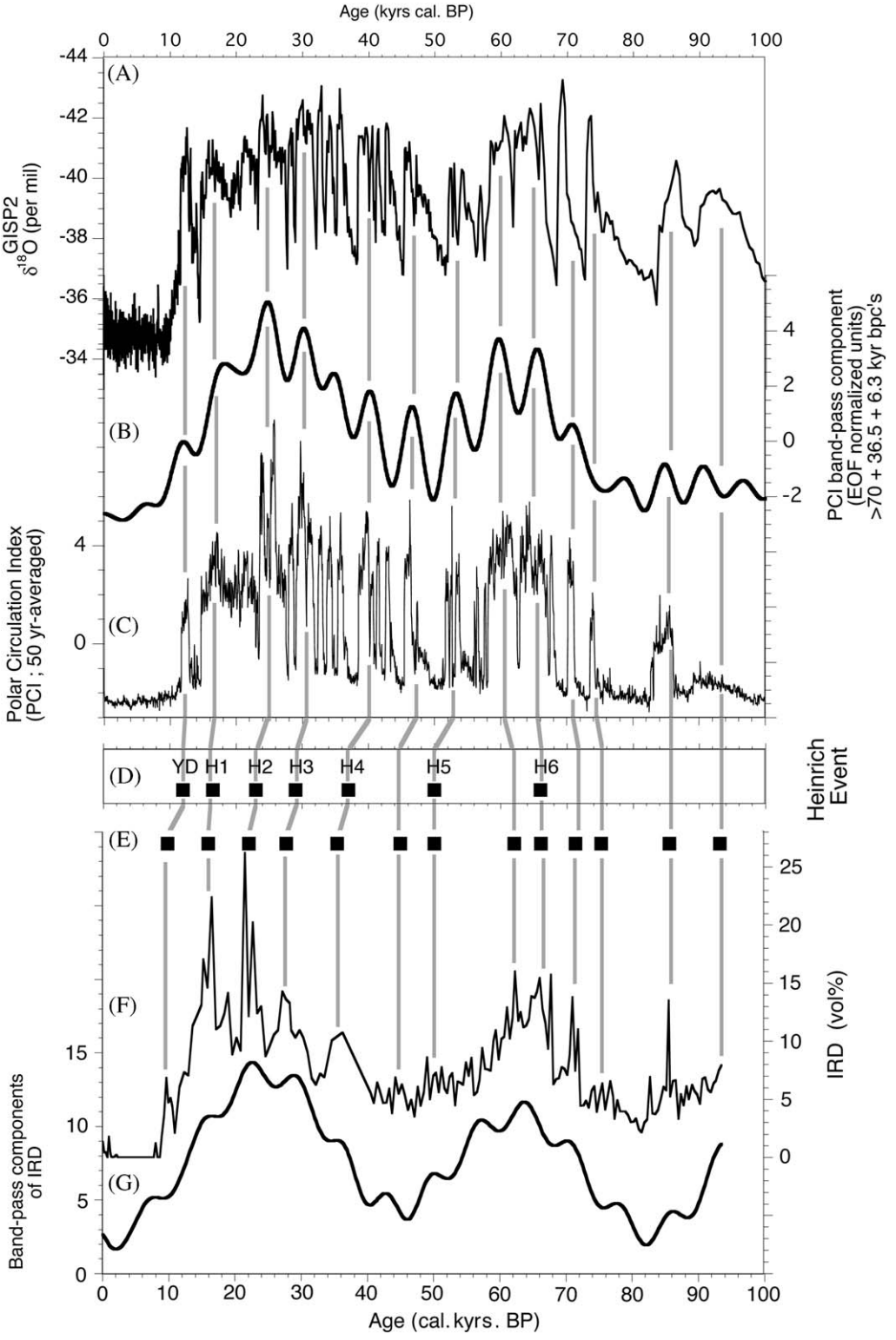
Age (kyrs cal. BP)
(A)
GISP2
δ18O (per mil)
(B)
PCI band-pass component
(EOF normalized units)
>70 + 36.5 + 6.3 kyr bpc's
(C)
Polar Circulation Index
(PCI ; 50 yr-averaged)
(D)
YD H1 H2 H3 H4 H5 H6
Heinrich
Event
(E)
(F)
IRD (vol%)
(G)
Band-pass components
of IRD
Age (cal. kyrs. BP)

During the past 100 kyrs, sea-ice has varied with both global and local climate changes. Sea-ice has expanded to the maximum state (Mode I) with short time intervals during the cold, glacial periods in MIS2 and 4 (Fig. 11E). During the transition from the late MIS5 to MIS 4, sea-ice was only found at the western Okhotsk Sea at ca. 80 ka, and then expanded to the central and western parts. In the late MIS4, sea-ice retreated from the western to central Okhotsk Sea at ca. 60 ka, with two short expansions during the early and middle MIS3. The minimum sea-ice situation (Mode III) occurred between 40 and 50 ka during the middle MIS3. During the last glaciation, sea-ice was found in the western Okhotsk Sea from ca. 40 to 36 ka, and rapidly increased in the entire Okhotsk Sea. During MIS2, high IRD sedimentation occurred in the eastern Okhotsk Sea much more significantly than in the previous cold interval of MIS4. During the last deglaciation, sea-ice began to retreat rapidly in the eastern Okhotsk Sea within a short period of time. Sudden westward regression occurred at 8 ka. Since approximately 8 ka IRD has been absent in the central part of the Okhotsk Sea.

Sea-ice expansion in the Okhotsk Sea has occurred not only during the glacial stages related to the Milankovitch time scale, but also during cold periods on the millennium time scale. We define these abrupt cooling events as the Okhotsk Sea-ice Expansion (OSIE) events. The estimated age of the OSIE are listed in Table 6. Spectral analyses of IRD variations in Core XP-PC2 indicate that these events occurred about 5–6-kyr intervals (5.8 and 5.1 kyrs), superimposed upon orbital-scale periodicities (78.7, 41.3, and 24.0 kyrs) (Fig. 12). Consequently, the long-term behavior of IRD deposition can be explained by the combination of the Milankovitch-forcing orbital cycles combined with the 5–6-kyr components.

5.4. Cause of millennium scale abrupt sea-ice expansion events in the Okhotsk Sea

Variation of IRD in the Okhotsk Sea appears to have obvious strong correlation with the Dansgaard-Oeschger (DO) fluctuations (Dansgaard et al., 1993; Bond et al., 1993) (Fig. 13). The timing of the OSIE events, represented by peaks of IRD series in Core XP-PC2, corresponds to millennium scale colder periods (stadials), represented by negative shifts of stable isotope ($\delta\ ^{18}O$) records in GRIP and GISP2 ice cores (White et al., 1997; Stuiver et al., 1995; Steig et al., 1994). Especially, the OSIE events simultaneously occurred at the peak timings of band-pass component of the Polar Circulation Index (PCI), which was based on an empirical orthogonal function (EOF) of the chemical series in the GISP2 ice cores (Fig. 13) (Mayewski et al., 1997). The PCI provides a relative measure of the average size and intensity of polar atmospheric circulation, because chemical compounds in the ice cores derived from sea salt and atmospheric dust increased during the stadials. Background variations and peaks of band-passed components of IRD series in Core XP-PC2, which contains 78.7, 41.3, 24.0, and 5.1-kyr periodicities, correspond to those of the PCI series, which contains >70, 36.5, and 6.3-kyr components (Figs. 12B and G). Mayewski et al. (1994) have attributed rapid climatic change to massive reorganization in atmospheric circulation, stimulated and sustained by changes in ocean ice cover. The sea-ice in the Okhotsk Sea, therefore, expanded in millennial time-scale under strong wind fields in enhanced polar atmospheric circulation during the stadial periods.

The majority of the OSIE events can be correlated to the timings of the Heinrich events (Heinrich, 1988; Bond et al., 1992), although some of those do not have counterparts. The Heinrich events, which have been recognized as the layers rich in IRD in the northern Atlantic sediment cores, are thought as a result from massive iceberg discharge and attendant cooling of surface waters in the northern Atlantic Ocean. Even though the different types of IRD events occur on both sides of the Northern Hemisphere, it seems that sea-ice expansion in the Okhotsk Sea directly responds to the PCI rather than the Heinrich events in the North Atlantic. The OSIE events show much more clear relationship with enhanced polar atmospheric circulation.

It is not possible to explain the reason why sea-ice expanded on two millennium scale in the Okhotsk Sea through the changes in global ocean thermohaline circulation. This is because that there are no millennium signals of biogenic opal in Core XP98-PC1 in the Okhotsk Sea, which is mainly related to upwelling of deep water (Narita et al., 2002). Therefore, massive changes in polar atmospheric circulation are a key process in explaining the cause of millennial abrupt and sudden expansion of sea-ice in the Okhotsk Sea. Atmospheric

circulation intensifaction during the cold period may emphasize atmospheric patterns for the Aleutian Low and Siberian High, resulting in strong wind fields over the Okhotsk region. This atmospheric forcing results in sea-ice expansion in the Okhotsk Sea.

6. Conclusions

By combining observations of IRD in settling particles, surface sediments, and sediment cores with satellite imagery, we have shown both modern and past processes associated with IRD accumulation in the Okhotsk Sea. Sediment trap experiments show processes involved in present-day IRD sedimentation and are used as a proxy for older examples. IRD, consisting of angular silt- and sand-sized particles, are released just after sea-ice melting in spring, as indicated by its, spatial distribution. The two dominant types of grain-size distributions within piston cores reflected spring and autumn fluxes. During the glacial periods, sea-ice expanded over the whole Okhotsk region, but it is unlikely that sea-ice cover was perennial. Before and after MIS 2 and 4, sea-ice gradually expanded eastward. Minimum sea-ice cover occurred between 40 and 50 kyrs, during MIS 3, and in the Holocene. During the last deglaciation, sea-ice began to retreat at the eastern margin of the Okhotsk Sea, and then suddenly regressed westward during the next 8 kyrs.

Sea-ice extent in the Okhotsk Sea has expanded rapidly and abruptly 13 times during the past 100 kyrs, which we term Okhotsk Sea Sea-ice Expansion (OSIE) events. The intensity of these events was amplified by continental ice sheet expansion during the glacials. The cause of these OSIE events was most likely related to a strengthening of the polar atmospheric circulation, Strong wind fields also played a major role in sea-ice expansion. Although, it remains to be explained why the polar atmospheric circulation intensified during millennial-scale stadials. Such forcing might be a result of external forcing, such as incoming solar radiation, or due to internal climatic dynamics. Future study is necessary to determine the nature of changing polar atmospheric circulation including sea-ice cover, which is a major contributor to climatic changes and which has important feedback effects on radiation balance in the atmosphere and the thermohaline circulation of the ocean.

Acknowledgments

This study was supported by a fund from Core Research for Evolutional Science and Technology (CREST), Japan Science and Technology Corporation. T. Sakamoto, T. Nakatsuka, and M. Wakatsuchi were funded by Grant-in-Aid for Scientific Research (No. 12440151) by the Ministry of Education, Culture, Sports, Science, and Technology, Japan.

References

Alfulis, M.A., Martin, S., 1987. Satellite passive microwave studies of Sea of Okhotsk ice cover and its relation to oceanic processes, 1978–1982. Journal of Geophysical Research 92, 13013–13028.

Bard, E., Arnold, M., Hamelin, B., Tisnerat-Laborde, N., Cabioch, G., 1998. Radiocarbon calibration by means of mass spectrometric $^{230}Th/^{234}U$ and ^{14}C ages of corals: an updated database including samples from Barbados, Mururoa and Tahiti. Radiocarbon 40, 1085–1092.

Bond, G., Heinrich, H., Broecker, W., Labeyrie, L., MacManus, J., Andrews, J., Huon, S., Jantschik, R., Clasen, S., Simet, C., Tedesco, K., Klas, M., Bonani, G., Ivy, S., 1992. Evidence for massive discharges of icebergs into the North Atlantic ocean during the last glacial period. Nature 360 (19), 245–249.

Bond, G., Broecker, W., Johnson, S., McManus, J., Labeyrie, L., Jouzel, J., Bonani, G., et al., 1993. Correlations between climate records from North Atlantic sediments and Greenland ice. Nature 365 (9), 143–147.

Borchardt, G.A., Aruscavage, P.J., Millard Jr., H.T., 1972. Correlation of the Bishop Ash, a Pleistocene marker bed, using instrumental neutron activation analysis. Journal of Sedimentary Petrology 42, 301–306.

Braitseva, O.A., Malekestev, I.V., Ponomareva, V.V., Sulerzhitsky, L.D., 1995. Ages of calderas, large explosive creters and active volcanoes in the Kuril-Kamchatka, Russia. Bulletin of Volcanology 57, 383–402.

Danhara, T., Yamashita, H., Kasuya, M., 1992. An improved system for measuring refractive index using the thermal immersion method. Quaternary International 13/14, 89–91.

Dansgaard, W., Johnsen, S.J., Clausen, H.B., Dahl-Jensen, D., Gundestrup, N.S., Hammer, C.U., Hvidberg, C.S., Steffensen, J.P., Sveinbjornsdottir, A.E., Jouzel, J., Bond, G., 1993. Evidence for general instability of past climate from a 250-kyr ice-cire record. Nature 364, 218–220.

Duplessy, J.C., Shakleton, N.J., Fairbanks, R.G., Labeirie, L., Oppo, D., Kallel, N., 1998. Deep water source variations during the last climatic cycle and their impact on the global deep water circulation. Paleocanography 3, 343–360.

Frenzel, B., Pesci, M., Velichko, A.A. (Eds.), 1992. Atlas of Paleoclimate and Paleoenvironments of the Northern Hemisphere: Late Pleistocene—Holocene. Geogr. Res. Inst., Hungarian Academy of Science, Budapest. Gustav Fischer Verlag, Stuttgart, Jena, New York 153pp.

Froggatt, P.C., 1983. Toward a comprehensive upper Quaternary tephra and ignimbrite stratigraphy in New Zealand using

electron microprobe analysis of glass shards. Quaternary Research 19, 188–200.

Gloerson, P., Champbell, W.J., Cavelieri, D.J., Comiso, C., Parkinson, C.L., Zwally, H.J., 1992. Arctic and Antarctic Sea-Ice, 1978–1987: Satellite Passive-Microwave Observations and Analysis, NASA Special Publication SP-511, 290pp.

Gorbarenko, S.A., 1996. Stable isotope and lithologic evidence of late Glacial and Holocene oceanography of the Northwestern Pacific and its marginal Seas. Quaternary Research 46, 230–250.

Gorbarenko, S.A., Khusid, T.A., Basov, I.A., Oba, T., Southon, J.R., Koizumi, I., 2002a. Glacial-Holocene environment of the southeastern Okhotsk Sea: evidence from geochemical and paleontological data. Palaeogeography, Palaeoclimatology, Palaeoecology 177, 237–263.

Gorbarenko, S.A., Nurnberg, D., Derkachev, A.N., Astakhov, A.S., Southon, J.R., Kaiser, A., 2002b. Magnetostratigraphy and tephrachronology of the upper quaternary sediments in the Okhotsk Sea: implications of terrigenous, volcanogenic and biogenic matter supply. Marine Geology 183, 107–129.

Gorbarenko, S.A., Leskov, V.Yu., Artemova, A.V., Tiedemann, R., Boebow, N., Nuernberg., D., 2003. Ice Cover of the Sea of Okhotsk during the Last Glaciation and Holocene. Doklady Earth Sciences 389, 208–211.

Heinrich, H., 1988. Origin and consequences of cyclic ice rafting in the northeast Atlantic Ocean during the past 130,000 years. Quaternary Research 29, 142–152.

Itoh, M., Oshima, I.Kay., Wakatsuchi, M., 2003. Distribution and formation of Okhotsk Sea Intermediate water: an analysis of isopycnal climatological data. Journal of Geophysical Research 108 (C8), 3258.

Itou, M., Ono, T., Noriki, S., 2003. Provenance of intermediate waters in the western North Pacific deduced from thermodynamic imprint on $\delta^{13}C$ of DIC. Journal of Geophysical Research 108 (C11), 3347.

Keigwin, L.D., 1998. Glacial age hydrography of the far northwest Pacific Ocean. Paleoceanography 13, 323–339.

Keigwin, L.D., Jones, G.A., Froelich, P.N., 1998. A 15000 year paleoenvironmental record from Meiji Seamount, far northwestern Pacific. Earth and Planetary Science Letters 111, 425–440.

Kimura, N., Wakatsuchi, M., 1999. Processes controlling the advance and retreat of sea-ice in the Sea of Okhotsk. Journal of Geophysical Research 104 (C5), 11137–11150.

Martinson, D.G., Pisias, N.G., Hays, J.D., Imblie, J., Moore Jr., T.c., Shackleton, N.J., 1987. Age dating and the orbital theory of the ice ages: development of a high-resolution 0 to 3000,000-year chronostratigraphy. Quaternary Research 27, 1–29.

Matsumoto, K., Oba, T., Lynch-Stieglitza, J., Yamamoto, H., 2002. Interior hydrography and circulation of the glacial Pacific Ocean. Quaternary Science Reviews 21, 1693–1704.

Mayewski, P.A., Meeker, L.D., Whitlow, SW., Twickler, M.S., Morrison, M.C., Bloomfield, P., Bond, G.C., Alley, R.B., Gow, A.J., Grootes, P.M., Meese, D.A., Ram, M., Taylor, K.C., Wumkes, W., 1994. Changes in atmospheric circulation and ocean ice cover over the North Atlantic during the last 41,000 years. Science 263, 1747–1751.

Mayewski, P.A., Meeker, L.D., Twickler, M.S., Whitlow, S.I., Yang, Q., Lyons, W.B., Prentice, M., 1997. Major features and forcing of high latitude northern hemisphere atmospheric circulation over the last 110,000 years. Journal of Geophysical Research 102 (C12), 26345–26366.

Morley, J.J., Hays, H.D., 1983. Oceanographic conditions associated with high abundance of the radiolarian *Cycladophora davisiana*. Earth Planetary Science Letters 66, 63–72.

Okazaki, Y., Takahashi, K., Nakatsuka, T., Honda, M.C., 2003. The production scheme of *Cycladophora davisiana* (Radiolaria) in the Okhotsk Sea and the northwestern North Pacific: implication for the paleoceanographic conditions during the glacials in the high latitude oceans. Geophysical Research Letters 30 (18), 1939.

Parkinson, C.L., Comiso, C., Zwally, H.J., Cavelieri, D.J., Gloerson, P., Champbell, W.J., 1987. Arctic Sea-Ice, 1973–1976: Satellite Passive-Microwave Observations, NASA Special Publication SP-489, 296pp.

Petschick, R., Kuhn, G., Gingle, F., 1996. Clay mineral distribution in surface sediments of the South Atlantic: sources, transport, and relation to oceanography. Marine Geology 130, 203–229.

Ponomareva, V.V., Kyle, P.R., Melekestsev, I.V., Rinkleff, P.G., Dirksen, O.V., Sulerzhitsky, L.D., Zaretskaia, N.E., Rourke, R., 2004. The 7600 (^{14}C) year BP Kurile Lake caldera-forming eruption, Kamchatka, Russia: stratigraphy and field relationships. Journal of Volcanology and Geothermal Research 136, 199–222.

Savoskul, O.S., 1999. Holocene Glacier Advances in the Headwaters of Sredniaya Avacha, Kamchatka, Russia. Quaternary Research 52, 14–26.

Shiga, K., Koizumi, I., 2000. Late Quaternary oceanographic changes in the Okhotsk Sea based on the diatom records. Marine Micropaleontology 38, 91–117.

Steig, E.J., Grootes, P.M., Stuiver, M., 1994. Seasonal precipitation timing and ice core records. Science 266, 1885–1886.

Stuiver, M., Grootes, P.M., Braziunas, T.F., 1995. The GISP2 ^{18}O climate record of the past 16,500 years and the role of the sun, ocean and volcanoes. Quaternary Research 44, 341–354.

Stuiver, M., Reimer, P.J., Bard, E., Beck, J.W., Burr, G.S., Hughen, K.A., Kromer, B., McCormac, G., van der Plicht, J., Spurk, M., 1998. INTCAL98 radiocarbon age calibration, 24,000-0 cal BP. Radiocarbon 40, 1041–1083.

Takahashi, K., 1998. The Bering and Okhotsk Seas: modern and past paleoceanographic changes and gateway impact. Journal of Asian Earth Sciences 16 (1), 49–58.

Talley, L.D., 1991. An Okhotsk Sea anomaly: implication for ventilation in the North Pacific. Deep-Sea Research 38, S171–S190.

Ternois, Y., Kawamura, K., Keigwin, L., Ohkouchi, N., 2000. Alkenone sea surface temperature in the Okhotsk Sea for the last 15 kyr. Geochemical Journal 34, 283–293.

Wakatsuchi, M., Martin, S., 1991. Water circulation in the Kuril Basin of the Okhotsk Sea and its relation to eddy formation. Journal of Oceanographic Society of Japan 47, 152–168.

Watanabe, T., Wakatsuchi, M., 1998. Formation of 26.8–26.9$\sigma\theta$ water in the Kuril Basin of the Sea of Okhotsk as possible origin of North Pacific intermediate water. Journal of Geophysical Research 103, 2849–2865.

White, J.W.C., Barlow, L.K., Fisher, D., Grootes, P.M., Jouzel, J., Johnsen, S.J., Stuiver, M., Clausen, H.B., 1997. The climate signal in the stable isotopes of snow from Summit, Greenland: results of comparisons with modern

climate observations. Journal of Geophysical Research 102, 26425–26439.

Yang, J., Honjo, S., 1996. Modeling the near-freezing dichothermal layer in the Sea of Okhotsk and its interannual variations. Journal of Geophysical Research 101, 16421–16433.

Zahn, R., Pederson, T.F., Bornhold, B.D., Mix, A.C., 1991. Water mass convection in the glacial subarctic Pacific (54°N, 148°W): physical constraints and the benthic-planktonic stable isotope record. Paleoceanography 6, 543–560.